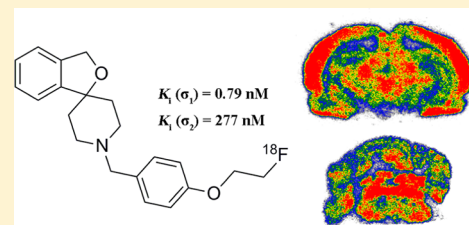


Synthesis and Evaluation of Novel  $^{18}\text{F}$ -Labeled Spirocyclic Piperidine Derivatives as  $\sigma_1$  Receptor Ligands for Positron Emission Tomography ImagingYan Li,<sup>†</sup> Xia Wang,<sup>†</sup> Jinming Zhang,<sup>‡</sup> Winnie Deuther-Conrad,<sup>§</sup> Fang Xie,<sup>†</sup> Xiaojun Zhang,<sup>‡</sup> Jian Liu,<sup>‡</sup> Jinping Qiao,<sup>†</sup> Mengchao Cui,<sup>†</sup> Jörg Steinbach,<sup>§</sup> Peter Brust,<sup>§</sup> Boli Liu,<sup>†</sup> and Hongmei Jia<sup>\*,†</sup><sup>†</sup>Key Laboratory of Radiopharmaceuticals (Beijing Normal University), Ministry of Education, College of Chemistry, Beijing Normal University, Beijing 100875, People's Republic of China<sup>‡</sup>Nuclear Medicine Department, Chinese PLA General Hospital, Beijing 100853, People's Republic of China<sup>§</sup>Helmholtz-Zentrum Dresden-Rossendorf, Institute of Radiopharmaceutical Cancer Research, Research Site Leipzig, Department of Neuroradiopharmaceuticals, 04318 Leipzig, Germany

## Supporting Information

**ABSTRACT:** A series of spirocyclic piperidine derivatives were designed and synthesized as  $\sigma_1$  receptor ligands. In vitro competition binding assays showed that 1'-(4-(2-fluoroethoxy)benzyl)-3H-spiro[2-benzofuran-1,4'-piperidine] (**19**) possessed high  $\sigma_1$  receptor affinity ( $K_i = 0.79$  nM) and excellent  $\sigma_1/\sigma_2$  subtype selectivity (350-fold) as well as high  $\sigma_1/\text{VACHT}$  selectivity (799-fold). The radiolabeled compound [ $^{18}\text{F}$ ]**19** was synthesized by substitution of the tosylate precursor **24** with [ $^{18}\text{F}$ ]fluoride, with an isolated radiochemical yield of 35–60%, a radiochemical purity of >99%, and a specific activity of 30–55 GBq/ $\mu\text{mol}$ . Biodistribution studies in imprinting control region mice indicated that [ $^{18}\text{F}$ ]**19** displayed excellent initial brain uptake and slow washout. Ex vivo autoradiography in Sprague–Dawley rats demonstrated high accumulation of the radiotracer in brain areas known to express high levels of  $\sigma_1$  receptors. Micro positron emission tomography imaging and blocking studies confirmed the specific binding of [ $^{18}\text{F}$ ]**19** to  $\sigma_1$  receptors in vivo.



## INTRODUCTION

$\sigma_1$  receptors, containing 223 amino acids with two trans-membrane domains, are a distinct class of intracellular membrane proteins.<sup>1–3</sup> They have a characteristic distribution in the central nervous system (CNS) and in peripheral organs such as the liver, spleen, lungs, heart, and kidneys.<sup>4,5</sup> The  $\sigma_1$  receptors function as “receptor chaperones” and are believed to be involved in the regulation of various ion channels, G-protein-coupled receptors, lipids, and other signaling proteins through a direct protein–protein interaction with another endoplasmic reticulum (ER) chaperone binding immunoglobulin protein/78 kDa glucose-regulated protein (BiP/GRP-78).<sup>2,3,6</sup> Recently, more and more evidence suggests that the  $\sigma_1$  receptors are implicated in a myriad of CNS diseases, such as anxiety, depression, schizophrenia, drug addiction, and Alzheimer's disease (AD).<sup>7–11</sup> In addition, the  $\sigma_1$  receptors are believed to be linked to a number of tumors as well as heart failure.<sup>12–14</sup>

Positron emission tomography (PET) and single-photon emission computed tomography (SPECT) are noninvasive imaging modalities useful in the investigation of receptor status in vivo. PET or SPECT imaging with  $\sigma_1$  receptor selective radiotracers could quantitatively visualize  $\sigma_1$  receptors in the living human brain, thus providing a valuable tool to investigate the function of this receptor and its dysregulation under diseased conditions. In the past few years, a number of PET

and SPECT imaging agents for  $\sigma_1$  receptors have been developed. Among these, [ $^{11}\text{C}$ ]SA4503 ([ $^{11}\text{C}$ ]**1**),<sup>15–19</sup> [ $^{18}\text{F}$ ]FPS ([ $^{18}\text{F}$ ]**2**),<sup>20,21</sup> and [ $^{123}\text{I}$ ]TPCNE ([ $^{123}\text{I}$ ]**3**)<sup>22</sup> (Figure 1) have been evaluated in human studies. However, [ $^{18}\text{F}$ ]**2** and [ $^{123}\text{I}$ ]**3** have been found to display irreversible kinetics and thus are not suitable for the quantification of  $\sigma_1$  receptors in vivo.<sup>20,22</sup> [ $^{11}\text{C}$ ]**1**, as the first useful PET radiotracer, showed high affinity for  $\sigma_1$  receptors and selectivity toward 36 other receptors, ion channels, and second messenger systems.<sup>23</sup> The in vivo [ $^{11}\text{C}$ ]**1** imaging studies showed that the density of  $\sigma_1$  receptors was decreased in the brain of Parkinson's disease (PD) and AD patients.<sup>15,16</sup> Due to the short half-life of  $^{11}\text{C}$  ( $t_{1/2} = 20$  min), use of [ $^{11}\text{C}$ ]**1** needs an on-site cyclotron. The longer half-life  $^{18}\text{F}$ -labeled compound seems more promising for  $\sigma_1$  receptor imaging.

In the past decade, a novel class of spirocyclic piperidine compounds were reported as potent  $\sigma_1$  receptor ligands. From this class compound **4** (1'-benzyl-3-methoxy-3H-spiro[2-benzofuran-1,4'-piperidine]; Figure 2) was shown to possess nanomolar affinity for  $\sigma_1$  receptors and excellent selectivity over the  $\sigma_2$  and more than 60 other receptors, transporters, and ion channels.<sup>24–26</sup> As a result, spirocyclic piperidines have been used as lead compounds to develop radiotracers for  $\sigma_1$  receptor

Received: November 25, 2012

Published: April 8, 2013

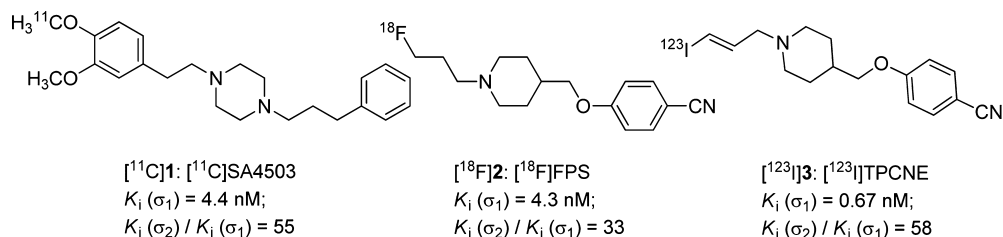


Figure 1. Structures of  $\sigma_1$  receptor radiotracers investigated in human studies.

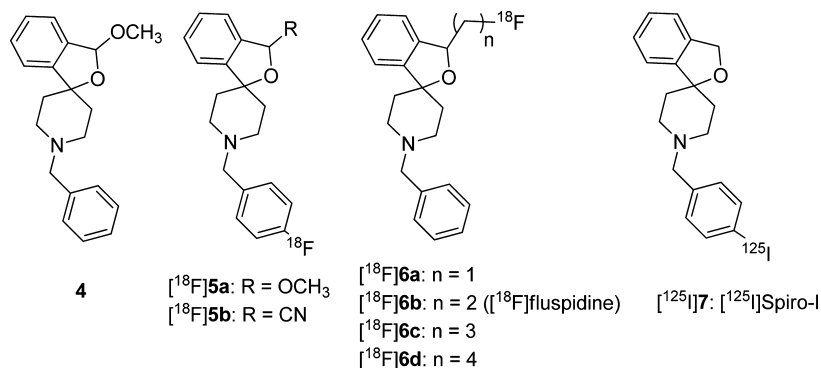


Figure 2. Spirocyclic piperidine  $\sigma_1$  receptor ligands and radiotracers.

imaging. The first approach in these development efforts was the direct incorporation of a fluorine atom into the benzene ring of the *N*-benzyl moiety (e.g., ligands  $[^{18}\text{F}]5a$  and  $[^{18}\text{F}]5b$ , Figure 2).<sup>27</sup> Unfortunately, these tracers were metabolically unstable in vivo and hence not suitable for imaging applications. The second approach was to introduce the fluorine atom into the C-3 side chain of the spirocyclic benzofuran system with a 1–4 carbon length (e.g.,  $[^{18}\text{F}]6$ , Figure 2).<sup>28–32</sup> From this approach,  $[^{18}\text{F}]fluspidine$  ( $[^{18}\text{F}]6b$ ) emerged as a potential radiotracer with favorable target affinity and specificity as well as as metabolic stability in vivo.

We took a third approach to the development of imaging agents from the spirocyclic piperidine series of compounds, i.e., structural modifications on the *N*-benzyl moiety while eliminating the substituent on the spirocyclic benzofuran section. We have previously reported the discovery of Spiro-I (7), with an iodine at the *para*-position of the benzyl moiety, as a ligand with high affinity and subtype selectivity for the  $\sigma_1$  receptors ( $\sigma_1$ ,  $K_i = 2.75 \text{ nM}$ ;  $\sigma_2$ ,  $K_i = 340 \text{ nM}$ ).<sup>33</sup> The radioligand  $[^{125}\text{I}]7$  (Figure 2) exhibited high initial brain uptake and specific binding to  $\sigma_1$  receptors in vivo. To develop a PET radiotracer as a  $\sigma_1$  receptor imaging agent with suitable properties, we replaced the iodine atom at the *para*-position of the *N*-benzyl moiety with either fluorine or a methoxy group for initial assessment of preserved affinity and selectivity. We also elongated the *para*-substituent with a short fluorooligoethoxylated chain (mono-, di-, and triethoxy) in an attempt to modify the affinity, lipophilicity, and pharmacokinetic properties of the resulting compounds. Moreover, we replaced the aromatic ring in the *N*-benzyl moiety with a pyridine group to further reduce the lipophilicity of this series of derivatives. The design concept is shown in Figure 3. Herein we report the synthesis and evaluation of spirocyclic piperidine derivatives as  $\sigma_1$  receptor ligands for imaging of  $\sigma_1$  receptor density in the brain.

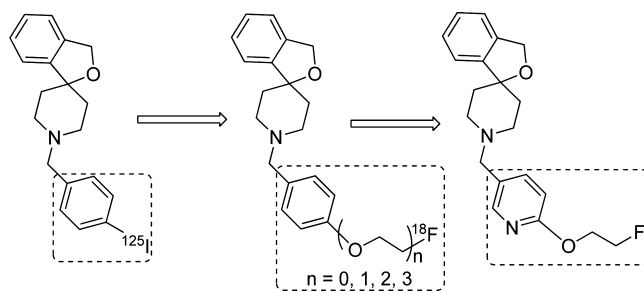
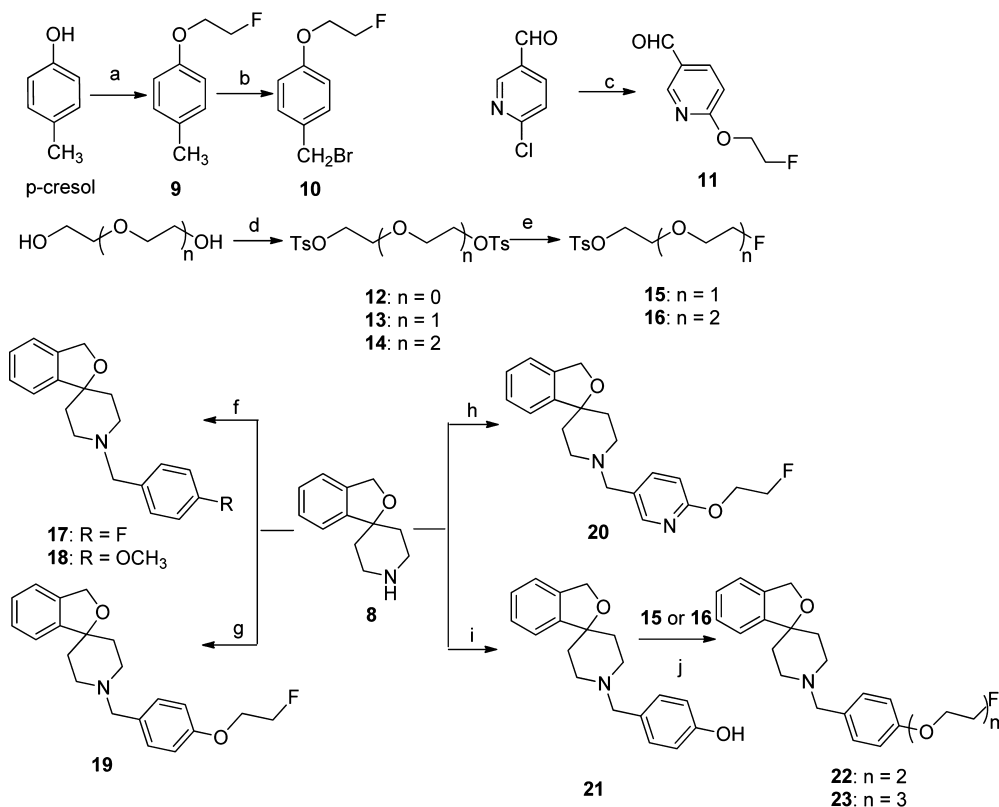


Figure 3. Design concept of  $^{18}\text{F}$ -labeled spirocyclic piperidine compounds.

## RESULTS

**Chemistry.** The synthetic routes for the novel spirocyclic piperidine ligands are depicted in Scheme 1. All compounds were prepared from the key intermediate **8** (3*H*-spiro[2-benzofuran-1,4'-piperidine]), which was synthesized according to a published method.<sup>34</sup> Preparation of intermediates **9** and **10** followed the method in the literature; i.e., *p*-cresol was reacted with 1-bromo-2-fluoroethane to obtain compound **9**, followed by radical bromination.<sup>35</sup> Another intermediate, 6-(2-fluoroethoxy)nicotinaldehyde (**11**), was obtained by reaction of 6-chloronicotinaldehyde with 2-fluoroethanol in the presence of *t*-BuOK in DMF. The intermediates **15** and **16** were obtained by fluorination of the oligoethylene glycol ditosylate esters **13** and **14** using anhydrous tetra-*n*-butylammonium fluoride (TBAF) in THF.<sup>36</sup> *N*-Alkylation of the intermediate **8** with 1-(bromomethyl)-4-fluorobenzene, 1-(bromomethyl)-4-methoxybenzene, or compound **10** provided compounds **17**, **18**, and **19**, respectively, with yields of 30%, 40%, and 57%. Reductive amination of compound **8** in the presence of  $\text{NaBH}(\text{OAc})_3$  with **11** or 4-hydroxybenzaldehyde led to the *N*-methylpyridinyl derivative **20** or compound **21**, respectively, with yields of 58% and 69%. The fluoroalkoxy analogues **22** and **23** were synthesized by heating the

Scheme 1. Synthetic Routes of Compounds 17–23<sup>a</sup>

<sup>a</sup>Reagents and conditions: (a) 1-bromo-2-fluoroethane, K<sub>2</sub>CO<sub>3</sub>, acetone, 60 °C, 10 h, 60%; (b) NBS, AIBN, CCl<sub>4</sub>, 80 °C, 4 h, 36%; (c) 2-fluoroethanol, *t*-BuOK, DMF, rt, 23%; (d) TsCl, KOH, CH<sub>2</sub>Cl<sub>2</sub>, 0 °C to rt, 75–80%; (e) TBAF (1 M in THF), THF, reflux, 42–58%; (f) K<sub>2</sub>CO<sub>3</sub>, KI, CH<sub>3</sub>CN; for 17, 1-(bromomethyl)-4-fluorobenzene, reflux, 30%; for 18, 1-(bromomethyl)-4-methoxybenzene, rt, 40%; (g) 10, NaH, THF, rt, 57%; (h) (i) 11, 1,2-dichloroethane, 2 h; (ii) NaBH(OAc)<sub>3</sub>, 6 h, 58%; (i) (i) 4-hydroxybenzaldehyde, 1,2-dichloroethane, 2 h; (ii) NaBH(OAc)<sub>3</sub>, 6 h, 69%; (j) CH<sub>3</sub>CN, K<sub>2</sub>CO<sub>3</sub>, reflux, 67% for 22, 74% for 23.

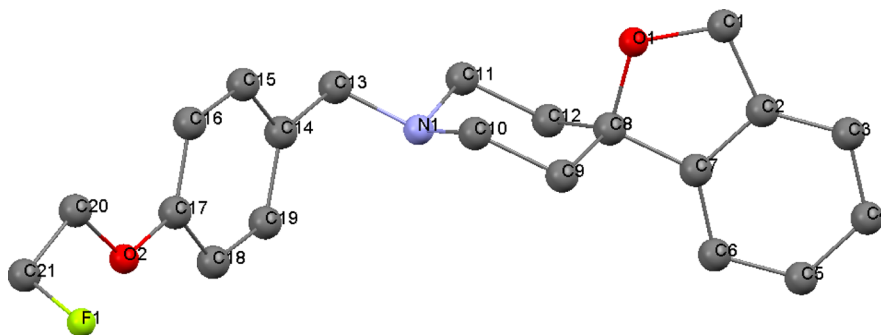


Figure 4. Crystal structure of compound 19.

intermediate 21 with tosylate derivatives 15 and 16 under basic condition (K<sub>2</sub>CO<sub>3</sub>) in acetonitrile with yields of 67% and 74%, respectively.

To examine the binding model of spirocyclic piperidine compounds, the single X-ray crystal structure analysis of compound 19 was carried out. Crystal data together with details of the determinations are summarized in the Supporting Information. The crystal structure with the atomic numbering scheme of compound 19 is shown in Figure 4. The oxygen atom of the benzofuran ring adopts the axial position at the piperidine chair. The distance between the N-atom and the center of the aromatic ring of the *N*-benzyl residue is 3.8 Å. The distance between the N-atom and the center of the aromatic ring of the benzofuran system is 5.7 Å.

**In Vitro Radioligand Competition Studies.** Affinities of the new compounds for the  $\sigma_1$  and  $\sigma_2$  receptors were determined in radioligand competition binding assays.<sup>37</sup> The results are listed in Table 1. In vitro competition binding assays indicated that, similarly to the previously reported spirocyclic piperidine derivatives,<sup>24,25</sup> small substituents at the *para*-position of the *N*-benzyl moiety, such as F, OCH<sub>3</sub>, or OCH<sub>2</sub>CH<sub>2</sub>F, preserved high affinity and selectivity for  $\sigma_1$  receptors (17–19). In particular, compound 19 exhibited subnanomolar affinity for  $\sigma_1$  receptors ( $K_i = 0.79 \pm 0.11$  nM) and excellent subtype selectivity ( $\sigma_2$  receptor,  $K_i = 277 \pm 71$  nM;  $K_i(\sigma_2)/K_i(\sigma_1) = 350$ ). Moreover, introduction of a fluoroethoxy group appeared to lead to an increase in subtype selectivity. On the other hand, substitution at the same position

**Table 1. Binding Affinities of the Spirocyclic Piperidine Derivatives toward  $\sigma_1$  and  $\sigma_2$  Receptors<sup>a</sup>**

compd	$K_i(\sigma_1)$ (nM)	$K_i(\sigma_2)$ (nM)	$K_i(\sigma_2)/K_i(\sigma_1)$
17 (Spiro-F)	0.58 ± 0.02	106 ± 21	182
Spiro-F <sup>b</sup>	0.18 ± 0.09	131	728
18	1.70 ± 1.74	276 ± 115	162
19	0.79 ± 0.11	277 ± 71	350
20	2.30 ± 0.69	327 ± 47	142
22	52.9 ± 2.33	860 ± 4.99	16
23	37.5 ± 2.54	592 ± 123	16
7 <sup>c</sup>	2.75 ± 0.12	340	123
haloperidol	4.95 ± 1.74	20.7 ± 0.07	4

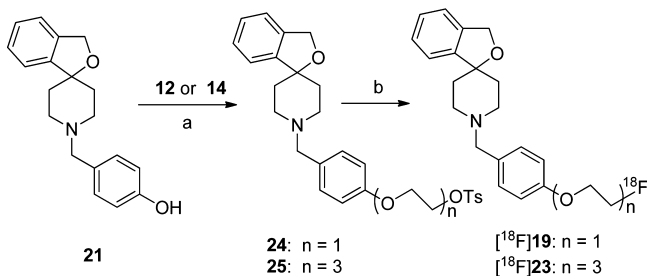
<sup>a</sup>Values are means ± SD of three experiments performed in triplicate.

<sup>b</sup>From ref 27. <sup>c</sup>From ref 33.

with an increased length of the fluorooligoethoxylated chain ( $n = 2, 3$ ) led to decreased affinities for  $\sigma_1$  receptors (compounds 22 and 23). Finally, replacement of the benzene ring with pyridine slightly decreased the affinity for  $\sigma_1$  receptors and subtype selectivity (20 vs 19).

Affinities of compound 19 for the vesicular acetylcholine transporter (VACHT) were also determined in radioligand competition binding assays.<sup>38</sup> Compound 19 exhibited low affinity for VACHT ( $K_i = 631 \pm 50.2$  nM) and thus resulted in excellent selectivity for  $\sigma_1$  receptors ( $K_i(\text{VACHT})/K_i(\sigma_1) = 799$ ).

**Radiochemistry.** The synthesis of the precursors and radioligands is outlined in Scheme 2. The tosylate precursors

**Scheme 2. Synthetic Route of the Precursors 24 and 25 and Radioligands [<sup>18</sup>F]19 and [<sup>18</sup>F]23<sup>a</sup>**

<sup>a</sup>Reagents and conditions: (a)  $\text{K}_2\text{CO}_3$ ,  $\text{CH}_3\text{CN}$ , reflux, 67% for 24, 61% for 25; (b) Kryptofix 2.2.2,  $\text{K}_2\text{CO}_3$ ,  $^{18}\text{F}^-$ ,  $\text{CH}_3\text{CN}$ , 95 °C, for [<sup>18</sup>F]19 35–60%, for [<sup>18</sup>F]23 20–40%.

24 and 25 were prepared from the coupling of 21 with ditosyl ethers 12 and 14 in yields of 67% and 61%, respectively. The formation of the desired compounds [<sup>18</sup>F]19 and [<sup>18</sup>F]23 was achieved through a direct S<sub>N</sub>2 displacement of the tosylate group in 24 and 25 with [<sup>18</sup>F]fluoride. After purification by semipreparative HPLC, [<sup>18</sup>F]19 and [<sup>18</sup>F]23 were obtained in 35–60% ( $n = 5$ ) and 20–40% ( $n = 3$ ) decay-corrected radiochemical yields, respectively, with a radiochemical purity (RCP) of >99%. The specific activity was 30–55 GBq/ $\mu\text{mol}$  at the end of the synthesis. The total synthesis time was about 1 h.

**Evaluation of Radiolabeled Compounds. Lipophilicity and in Vitro Stability.** For compounds 19 and 23, calculated log  $P$  (clog $P$ ) values obtained by the Chemdraw software are 3.14 and 2.83, respectively, lower than those of compounds from the [<sup>18</sup>F]6 series (clog $P$  of 3.25–4.23 for 6a–6d, Figure 2).<sup>32</sup> The log  $D_{7.4}$  values of the two radiotracers [<sup>18</sup>F]19 and [<sup>18</sup>F]23 were determined using a shake flask method.<sup>39</sup> The log

$D_{7.4}$  values for [<sup>18</sup>F]19 and [<sup>18</sup>F]23 were  $2.41 \pm 0.09$  and  $1.90 \pm 0.06$ , respectively (Table 2), indicating that the lipophilicity of the radiotracers decreases with the introduction of extra ethoxy units at the *para*-position of the *N*-benzyl moiety.

The in vitro stability of [<sup>18</sup>F]19 was evaluated by measuring the RCP under different conditions. [<sup>18</sup>F]19 proved to be chemically stable in 0.9% NaCl solution and in 80% ethanol at room temperature for up to 4 h. Furthermore, after incubation with mouse plasma at 37 °C for 4 h, [<sup>18</sup>F]19 retained a RCP of >99%, indicating an excellent stability in vitro.

**Biodistribution Studies in Mice and Blocking Studies.** To evaluate the pharmacokinetics of the two radiotracers [<sup>18</sup>F]19 and [<sup>18</sup>F]23, biodistribution studies were performed in male imprinting control region (ICR) mice at 2, 30, 60, and 120 min postinjection. The results are presented in Table 2. [<sup>18</sup>F]19 displayed high initial brain uptake and a slow clearance rate with 8.07% injected dose (ID)/g at 2 min, 9.32% ID/g at 30 min, and 8.99% ID/g at 120 min. Among peripheral organs, the liver displayed a kinetic profile similar to that in the brain, with peak uptake of 15.30% ID/g at 30 min. The lungs and heart exhibited a significantly high uptake at 2 min (47.91% and 21.71% ID/g, respectively), which decreased gradually (16.20% and 8.54% ID/g at 120 min, respectively). The high uptake in these organs is consistent with the expression of  $\sigma_1$  receptors and similar to the tissue distribution pattern of [<sup>18</sup>F]6b.<sup>3f</sup>

Compared with [<sup>18</sup>F]19, [<sup>18</sup>F]23 displayed lower brain uptake and relatively fast washout with 5.79% ID/g at 2 min and 3.91% ID/g at 120 min following tracer injection. [<sup>18</sup>F]23 also showed similarly fast washout in the peripheral organs known to contain  $\sigma_1$  receptors, such as the lungs and kidneys, which may reflect the lower affinity of this radiotracer for  $\sigma_1$  receptors. In addition, accumulation of [<sup>18</sup>F]19 and [<sup>18</sup>F]23 in the bone increased only slightly over time, suggesting that defluorination was minimal in mice and that both radiotracers were fairly stable in vivo.

To detect the specific binding of [<sup>18</sup>F]19 to  $\sigma_1$  receptors in vivo, the effects of preinjection of haloperidol (0.1 mL, 1.0 mg/kg) on the biodistribution of radioactivity in various organs of male ICR mice were examined. Either saline or haloperidol was injected 5 min prior to the radiotracer injection. The results of blocking studies at 60 min postinjection are listed in Table 3. A significant reduction of 58% ( $p < 0.001$ ) in the accumulation of radiotracer was observed in the brain. Moreover, accumulation of radiotracer in other organs known to contain  $\sigma_1$  receptors was also significantly reduced by haloperidol pretreatment (reduction of 61%, 76%, 47%, and 64% in the heart, lungs, kidneys, and liver, respectively). The same blocking study was carried out with [<sup>18</sup>F]23. Little reduction in radiotracer accumulation was seen in the brain (16%). These results demonstrated that specific binding of this radiotracer is small, reflecting its lower affinity for  $\sigma_1$  receptors.

On the basis of the results reported in the literature, compound 1 had weak binding affinities for  $\alpha_1$  adrenergic, dopamine D<sub>2</sub>, serotonin (5-HT)<sub>1A</sub>, 5-HT<sub>2</sub>, histamine H<sub>1</sub>, muscarinic M<sub>1</sub>, and muscarinic M<sub>2</sub> receptors at a concentration of 10  $\mu\text{M}$ . However, these binding affinities were about 100 times lower than that for the  $\sigma_1$  receptor subtype. 1 had no affinity for 29 other receptors, ion channels, and second messenger systems.<sup>23</sup> These data indicated that 1 is a better  $\sigma_1$  receptor ligand for demonstrating the specificity of the novel ligands compared to haloperidol. To further investigate the specific binding of [<sup>18</sup>F]19 to  $\sigma_1$  receptors in vivo, blocking studies were carried out by preinjection of different

Table 2. Biodistribution of Radiotracers [ $^{18}\text{F}$ ]19 and [ $^{18}\text{F}$ ]23 in Male ICR Mice<sup>a</sup>

organ	2 min	30 min	60 min	120 min
		[ $^{18}\text{F}$ ]19 (log $D = 2.41 \pm 0.09$ )		
blood	1.71 $\pm$ 0.26	0.72 $\pm$ 0.12	0.80 $\pm$ 0.08	1.20 $\pm$ 0.15
brain	8.07 $\pm$ 1.00	9.32 $\pm$ 0.50	9.10 $\pm$ 0.60	8.99 $\pm$ 0.37
heart	21.71 $\pm$ 2.57	14.39 $\pm$ 1.51	10.74 $\pm$ 1.31	8.54 $\pm$ 0.36
liver	8.46 $\pm$ 0.55	15.30 $\pm$ 2.14	13.87 $\pm$ 1.80	13.60 $\pm$ 1.09
spleen	4.84 $\pm$ 0.52	8.20 $\pm$ 1.82	8.52 $\pm$ 0.89	9.09 $\pm$ 0.93
lung	47.91 $\pm$ 8.41	25.89 $\pm$ 3.30	25.21 $\pm$ 6.99	16.20 $\pm$ 1.59
kidney	18.76 $\pm$ 2.04	13.16 $\pm$ 1.80	10.87 $\pm$ 1.29	9.55 $\pm$ 0.80
stomach <sup>b</sup>	1.45 $\pm$ 0.22	1.09 $\pm$ 0.21	0.90 $\pm$ 0.12	0.89 $\pm$ 0.10
intestine <sup>b</sup>	6.62 $\pm$ 0.57	8.02 $\pm$ 0.38	7.81 $\pm$ 0.67	7.17 $\pm$ 0.94
muscle	5.45 $\pm$ 0.44	4.59 $\pm$ 0.44	4.41 $\pm$ 0.88	4.01 $\pm$ 0.54
bone	2.74 $\pm$ 0.63	3.30 $\pm$ 0.15	4.27 $\pm$ 0.49	6.13 $\pm$ 0.86
brain/blood	4.7	12.9	11.4	7.5
		[ $^{18}\text{F}$ ]23 (log $D = 1.90 \pm 0.06$ )		
blood	1.97 $\pm$ 0.23	2.96 $\pm$ 0.15	3.35 $\pm$ 0.36	3.52 $\pm$ 1.40
brain	5.79 $\pm$ 0.76	5.20 $\pm$ 0.32	4.63 $\pm$ 0.65	3.91 $\pm$ 0.74
heart	7.69 $\pm$ 0.69	2.95 $\pm$ 0.37	3.43 $\pm$ 0.38	3.25 $\pm$ 0.37
liver	5.83 $\pm$ 0.75	8.67 $\pm$ 0.82	6.32 $\pm$ 0.76	4.14 $\pm$ 0.68
spleen	5.35 $\pm$ 1.25	7.64 $\pm$ 0.79	5.43 $\pm$ 0.91	3.91 $\pm$ 0.93
lung	20.68 $\pm$ 1.55	4.46 $\pm$ 0.36	3.73 $\pm$ 0.40	3.16 $\pm$ 0.35
kidney	16.45 $\pm$ 1.56	5.09 $\pm$ 0.45	4.37 $\pm$ 0.70	3.96 $\pm$ 0.91
stomach <sup>b</sup>	2.19 $\pm$ 0.26	2.00 $\pm$ 0.64	1.45 $\pm$ 0.52	2.03 $\pm$ 0.35
intestine <sup>b</sup>	6.21 $\pm$ 0.97	6.72 $\pm$ 1.13	4.68 $\pm$ 0.48	4.04 $\pm$ 0.96
muscle	3.22 $\pm$ 0.57	2.42 $\pm$ 0.36	2.64 $\pm$ 0.26	2.62 $\pm$ 0.34
bone	3.38 $\pm$ 0.79	4.10 $\pm$ 0.52	4.51 $\pm$ 0.51	5.28 $\pm$ 1.49
brain/blood	2.9	1.8	1.4	1.1

<sup>a</sup>Data are expressed as percentage of injected dose per gram, mean  $\pm$  SD,  $n = 5$ . <sup>b</sup>Percentage of injected dose per organ.

concentrations of **1** (2, 5, or 10  $\mu\text{mol/kg}$ ) 5 min prior to the radiotracer injection. Blocking results of organ distribution of [ $^{18}\text{F}$ ]19 at 60 min postinjection in ICR mice are summarized in Figure 5A. Pretreatment of animals with different concentrations of **1** resulted in a significant reduction in radiotracer uptake in organs known to contain  $\sigma_1$  receptors, including the brain (46–56%), heart (60–63%), lungs (71–76%), kidneys (57–64%), and spleen (29–55%). Moreover, with pretreatment of animals with a higher concentration of **1**, higher reduction of radiotracer accumulation was observed in organs known to contain  $\sigma_1$  receptors. At the same time, higher radiotracer accumulation was observed in blood. Since our aim is to develop  $\sigma_1$  receptor ligands for imaging  $\sigma_1$  receptor density in the brain, we also use other receptor ligands, including tamoxifen (a ligand with high affinity for the emopamil binding protein (EBP) receptor), (*S*)-(-)-raclopride (dopamine  $D_2/D_3$  receptor ligand), or fluvoxamine (SSRI) as well as haloperidol and **1**, as blocking agents. The blocking results in the brain are presented in Figure 5B. In contrast with haloperidol and **1**, no significant reduction was observed by preinjection of tamoxifen, (*S*)-(-)-raclopride, and fluvoxamine, indicating that [ $^{18}\text{F}$ ]19 does not bind to EBP, dopamine  $D_2/D_3$  receptors, and serotonin transporter (5-HTT) in the brain at the low doses used for imaging.

**Ex Vivo Autoradiography in Sprague–Dawley Rats.** To investigate the accumulation of [ $^{18}\text{F}$ ]19 in different brain regions, an ex vivo autoradiography study was carried out in Sprague–Dawley rats. The results are presented in Figure 6. It is notable that a distinctly high accumulation was observed in the cortex, especially in the temporal cortex auditory area (TeAud). The accumulation was a little lower in the primary visual cortex. Moderate accumulation of radiotracer was

observed in the hypothalamus and thalamus. As presented in Figure 6, there was no remarkable higher accumulation in the hippocampus. There was negligible uptake of [ $^{18}\text{F}$ ]19 in the lateral ventricle and white matter (internal capsule). In the cerebellum, regions with comparably high uptake (vermian lobule) and comparably low uptake (paramedian lobule) were observed. Taken together, the distribution of [ $^{18}\text{F}$ ]19 in the rat brain is consistent with the density profile of  $\sigma_1$  receptors. To compare our results with those of [ $^{11}\text{C}$ ]1,<sup>40</sup> we selected the cerebellum as a reference region and calculated the region to cerebellum activity ratios for both tracers. The results are shown in Table 4. The rank order of [ $^{18}\text{F}$ ]19 uptake in various brain regions is in good agreement with that of [ $^{11}\text{C}$ ]1. When the results of [ $^{18}\text{F}$ ]19 were compared with those of [ $^{18}\text{F}$ ]6b,<sup>31</sup> where ex vivo autoradiography was performed in the brain of the CD-1 mouse, both radiotracers displayed high accumulation in the cerebellum, cortex, and superficial gray layer of the superior colliculus and moderate accumulation in the hippocampus. However, [ $^{18}\text{F}$ ]6b showed an extremely high accumulation in the facial nucleus, while moderate accumulation in this region was found for [ $^{18}\text{F}$ ]19. The accumulation of [ $^{18}\text{F}$ ]19 in the cortex and thalamus is slightly higher than that of [ $^{18}\text{F}$ ]6b.

**MicroPET Studies.** To further evaluate the in vivo distribution of [ $^{18}\text{F}$ ]19 and confirm its specific binding to  $\sigma_1$  receptors, microPET/computed tomography (CT) studies were carried out in anaesthetized Sprague–Dawley rats. In vivo binding specificity was evaluated in a blocking study with preadministration of haloperidol (1 mg/kg) 5 min prior to radiotracer injection. Sagittal and coronal brain images at 60 min postinjection of the tracer are shown in Figure 7. [ $^{18}\text{F}$ ]19 crossed the blood–brain barrier (BBB) rapidly and accumu-

**Table 3.** Effects of Preinjection of Haloperidol (0.1 mL, 1.0 mg/kg) 5 min Prior to the Injection of Radiotracer [ $^{18}\text{F}$ ]19 or [ $^{18}\text{F}$ ]23 on the Biodistribution of Radioactivity in Male ICR Mice<sup>a</sup>

organ	60 min (control)	60 min (blocking)	blocking (%)	<i>p</i> <sup>b</sup>
		<b>[<math>^{18}\text{F}</math>]19</b>		
blood	0.94 ± 0.37	4.25 ± 0.70	352	<0.001
brain	9.65 ± 0.70	4.06 ± 0.65	-58	<0.001
heart	10.15 ± 1.29	3.99 ± 0.53	-61	<0.001
liver	15.86 ± 2.21	5.72 ± 0.80	-64	<0.001
spleen	8.36 ± 0.17	8.75 ± 1.21	5	0.611
lung	23.92 ± 1.73	5.71 ± 0.96	-76	<0.001
kidney	10.79 ± 0.87	5.69 ± 1.02	-47	<0.001
stomach <sup>c</sup>	1.09 ± 0.20	3.36 ± 0.67	208	0.001
intestine <sup>c</sup>	7.38 ± 1.20	6.85 ± 2.02	-7	0.699
muscle	4.27 ± 0.17	3.41 ± 0.51	-20	0.032
bone	4.69 ± 0.01	5.54 ± 0.88	18	0.254
		<b>[<math>^{18}\text{F}</math>]23</b>		
blood	3.84 ± 0.22	4.51 ± 0.36	17	0.013
brain	4.51 ± 0.89	3.80 ± 0.51	-16	0.171
heart	3.39 ± 0.42	3.97 ± 0.70	17	0.245
liver	5.61 ± 1.27	3.61 ± 0.29	-36	0.010
spleen	6.50 ± 1.28	4.40 ± 0.32	-32	0.009
lung	3.72 ± 0.43	3.93 ± 0.34	6	0.432
kidney	4.07 ± 0.64	4.53 ± 0.36	11	0.216
stomach <sup>c</sup>	2.16 ± 0.19	2.77 ± 0.92	28	0.314
intestine <sup>c</sup>	4.83 ± 0.21	6.30 ± 0.56	30	0.006
muscle	2.99 ± 0.23	3.51 ± 0.63	17	0.159
bone	6.47 ± 1.04	4.79 ± 0.73	-26	0.024

<sup>a</sup>Data are expressed as percentage of injected dose per gram, mean ± SD, *n* = 5. <sup>b</sup>Values for the control versus blocking group at 60 min postinjection by Student's *t* test (independent, two-tailed). <sup>c</sup>Percentage of injected dose per organ.

lated in the midbrain, thalamus, and hypothalamus. High uptakes were also seen in the cortex, pontine reticular nucleus, and cerebellum. Lower uptakes were observed in the internal capsule and olfactory bulb, areas with negligible levels of  $\sigma_1$  receptors and thus a representation of nonspecific binding. When rats were pretreated with haloperidol, uptake levels of

[ $^{18}\text{F}$ ]19 decreased in all brain regions, consistent with the results from the biodistribution study.

**Additional Biological Studies. In Vitro Metabolism of Compound 19 by Rat Liver Microsomes.** Metabolites of compound 19 in the rat liver microsomes were determined by ultraperformance liquid chromatography (UPLC)–MS. They were identified by comparing the incubation samples with the blank samples (incubation in the absence of 19). Figure 8 presents the total ion chromatography (TIC) of metabolites from compound 19 incubated with rat liver microsomes at 37 °C for 30 min. Three metabolites were observed. The retention time of compound 19 was 1.82 min. Metabolites M1 and M2 eluted at 1.74 and 1.28 min, respectively. Metabolite M1 showed a protonated molecular ion at *m/z* 296, a loss of 46 Da from the parent molecule, suggesting an *O*-dealkylated product. Metabolite M2 displayed a protonated molecular ion of *m/z* 358, an increase of 16 Da from the parent molecule. Since M2 eluted off earlier than both M1 and the parent, it was postulated as an oxidized species of the parent. The third metabolite M3 presented a protonated molecular ion of *m/z* 360, an increase of 18 Da from 19, with a retention time of 1.42 min, so metabolite M3 was considered as the furan ring-opening product. The proposed metabolic pathways for ligand 19 are given in Figure 8.

**In Vivo Metabolic Stability of [ $^{18}\text{F}$ ]19.** The metabolic fate of [ $^{18}\text{F}$ ]19 was investigated in the brain and liver of male ICR mice 30 min after administration of the radiotracer. Figure 9 shows that the parent compound [ $^{18}\text{F}$ ]19 was the only radioactive species present in the mouse brain, indicating no entry of radioactive metabolites into the brain. HPLC analyses of mouse liver extract revealed two less lipophilic radiometabolites, which correspond to the two F-containing metabolites found from the metabolic studies with microsomes in vitro. The retention times of the parent tracer and these two radiometabolites are 7.72 min (40.3%), 5.70 min (32.8%), and 4.68 min (26.9%), respectively.

## DISCUSSION AND CONCLUSION

Neuroimaging with  $\sigma_1$  receptor PET radiotracers provides an important tool to investigate the involvement of this receptor subtype in the pathophysiology of neuropsychiatric diseases such as schizophrenia, depression, anxiety, and dementia.<sup>9,11,41</sup>

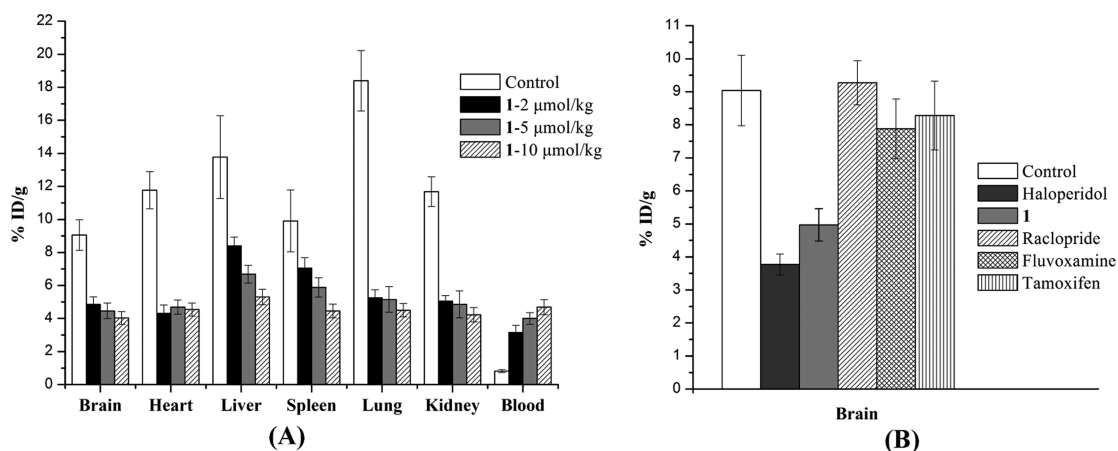


**Figure 5.** (A) Effects of preinjection of different concentrations of 1 (2, 5, or 10  $\mu\text{mol/kg}$ ) on organ distribution of [ $^{18}\text{F}$ ]19 (370 kBq, 0.1 mL) 60 min after intravenous injection. Student's *t* test was performed, and *p* < 0.05. (B) Effects of preinjection of haloperidol, 1, (S)-(-)-raclopride, fluvoxamine, or tamoxifen (2.2  $\mu\text{mol/kg}$ ) on brain accumulation of [ $^{18}\text{F}$ ]19. Student's *t* test was performed, and *p* < 0.001 for haloperidol and 1.

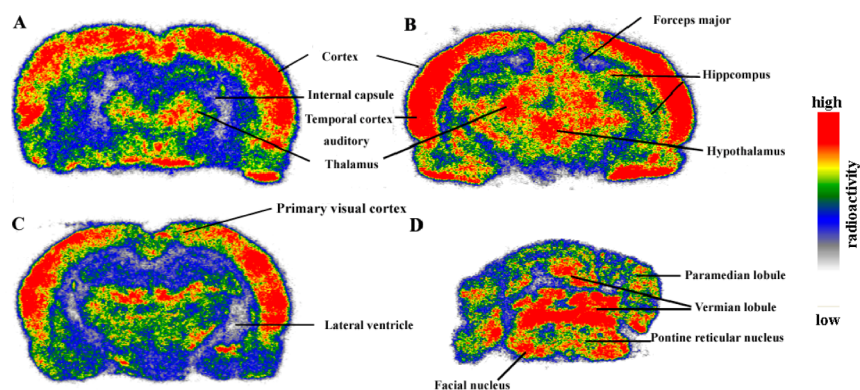


**Figure 6.** Ex vivo autoradiography of coronal brain slices of the rat brain obtained 60 min after intravenous injection of [ $^{18}\text{F}$ ]19 (12.2 MBq, 0.2 mL). (A), (B), (C), and (D) are the slices from the anterior to the posterior.

**Table 4. Comparison of the ex Vivo Autoradiography Results of [ $^{18}\text{F}$ ]19 with Those of [ $^{11}\text{C}$ ]1<sup>a</sup>**

region	[ $^{11}\text{C}$ ]1	[ $^{18}\text{F}$ ]19	region	[ $^{11}\text{C}$ ]1	[ $^{18}\text{F}$ ]19
TeAud	2.06	1.90	thalamus	1.70	1.38
frontal cortex	1.59	1.50	hippocampus	0.96	1.22
interior colliculus	1.78	1.30			

<sup>a</sup>Uptakes of [ $^{11}\text{C}$ ]1 and [ $^{18}\text{F}$ ]19 in each region are expressed as ratios (with the cerebellum as the reference region).

Since spirocyclic piperidine compound **4** possessed nanomolar affinity for  $\sigma_1$  receptors and excellent selectivity over the  $\sigma_2$  and more than 60 other receptors, transporters, and ion channels,<sup>24–26</sup> we use this compound as the lead compound to develop radiotracers for  $\sigma_1$  receptor imaging. In our previous work, we introduced iodine at the *para*-position of the benzyl moiety and found compound **7** possessed high affinity and subtype selectivity for the  $\sigma_1$  receptors.<sup>33</sup> In addition, the radioligand [ $^{125}\text{I}$ ]7 exhibited high initial brain uptake and specific binding to  $\sigma_1$  receptors in vivo. Therefore, to develop a suitable PET radiotracer as a  $\sigma_1$  receptor imaging agent, we replaced the iodine atom at the *para*-position of the *N*-benzyl moiety with fluorine, a methoxy group, and a short fluorooligoethoxylated chain (mono-, di-, and triethoxy). The single X-ray crystal structure analysis of compound **19** showed that the oxygen atom of the benzofuran ring adopted the axial position at the piperidine chair, which confirmed the calculation results by Rack et al. that the conformation with the oxygen atom in the axial orientation was more stable than that with the oxygen atom in the equatorial orientation.<sup>42</sup> The distance between the N-atom and the center of the aromatic ring of the *N*-benzyl residue is exactly within the range of the  $\sigma_1$  receptor pharmacophore model postulated by Glennon (2.5–3.9 Å).<sup>43</sup>

The distance between the N-atom and the center of the aromatic ring of the benzofuran system is a little shorter than the postulated distance based on Glennon's pharmacophore model (6–10 Å).

In vitro binding assay showed that all new compounds displayed selective binding to the  $\sigma_1$  receptors. Among them, compound **19** possessed the highest affinity and subtype selectivity for  $\sigma_1$  receptors. Moreover, compound **19** displayed 799-fold less affinity for VAcHT. Thus, compound **19** is a more promising  $\sigma_1$  receptor ligand compared to **17** and **7**. To define the lower affinity limit of a ligand for imaging of  $\sigma_1$  receptors and to detect the pharmacokinetics profile of the influence of the oligoethoxylated chain, we decided to carry out the radiolabeling of **19** and **23** with  $^{18}\text{F}$  and evaluation of the corresponding  $^{18}\text{F}$ -labeled radiotracers [ $^{18}\text{F}$ ]19 and [ $^{18}\text{F}$ ]23 for in vitro and in vivo studies.

For in vitro properties, the lipophilicity of the radioligand is important in the development of brain PET tracers. Moderate lipophilicity ( $\log D = 1–3$ ) is considered desirable for adequate blood–brain barrier penetration, increased free (protein-unbound) fraction in the plasma, and decreased nonspecific binding in the brain, which all lead to increased brain uptake and enhanced specific binding signals.<sup>44,45</sup> For compounds **19** and **23**,  $\text{clogP}$  values obtained by the Chemdraw software are lower than those of compounds from the [ $^{18}\text{F}$ ]6b series.<sup>32</sup> In addition, the lipophilicity of [ $^{18}\text{F}$ ]19 and [ $^{18}\text{F}$ ]23 is lower than that of [ $^{125}\text{I}$ ]7 ( $\log D_{7,4} = 3.06 \pm 0.11$ ).<sup>33</sup> The lipophilicity of [ $^{18}\text{F}$ ]19 and [ $^{18}\text{F}$ ]23 is within the optimal range for adequate brain entry and reduced nonspecific binding to brain tissue. Furthermore, [ $^{18}\text{F}$ ]19 displayed remarkable stability in vitro at room temperature for up to 4 h.

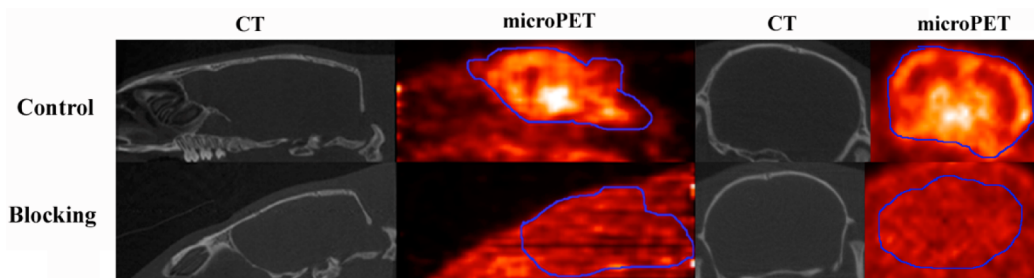


**Figure 7.** Sagittal and axial CT and microPET images in rats. PET images are summed from 60 to 90 min after intravenous injection with [ $^{18}\text{F}$ ]19 (23 MBq, 0.2 mL) under control and blocking conditions.

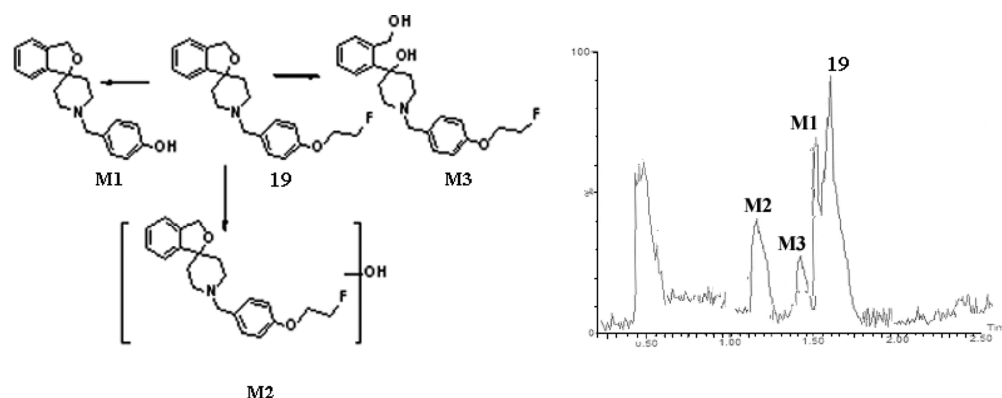


**Figure 8.** Proposed metabolic pathways of compound **19** in rat liver microsomes (left) and total ion chromatography recorded after incubation of compound **19** with rat liver microsomes at 37 °C for 30 min (right).

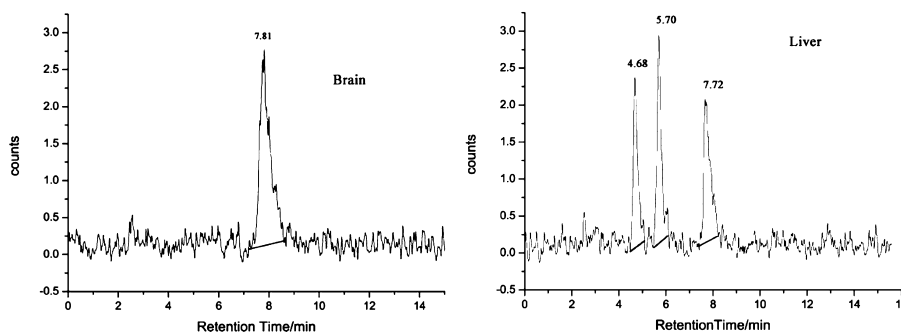


**Figure 9.** Analytical HPLC chromatograms of the mouse brain (left) and liver (right) extracts, taken 30 min after administration of [ $^{18}\text{F}$ ]**19** (18.5 MBq, 0.2 mL).

Following these encouraging *in vitro* properties, biological experiments were carried out to evaluate the labeled compounds for their potential as PET imaging tracers. In biodistribution studies in mice, the brain uptake of [ $^{18}\text{F}$ ]**19** (9.32% ID/g at 30 min) is higher than that of [ $^{11}\text{C}$ ]**1** (3.61% ID/g at 5 min),<sup>46</sup> [ $^{18}\text{F}$ ]**6b** (3.88% ID/g at 5 min),<sup>31</sup> or [ $^{125}\text{I}$ ]**7** (5.28% ID/g at 15 min).<sup>33</sup> [ $^{18}\text{F}$ ]**19** also exhibited a high brain-to-blood ratio of 12.9 at 30 min postinjection, which is comparable to that of [ $^{11}\text{C}$ ]**1** (11.6 at 30 min)<sup>46</sup> but somewhat lower than that of [ $^{18}\text{F}$ ]**6b** (18.8 at 120 min).<sup>31</sup> It needs to be pointed out that [ $^{18}\text{F}$ ]**19** displayed little defluorination *in vivo*, which is also important in  $^{18}\text{F}$ -labeled tracer development.

Currently, haloperidol is the most widely used  $\sigma_1$  antagonist in research on  $\sigma_1$  receptors, and its affinity is high enough to bind  $\sigma_1$  receptors in humans and small animals. Therefore, in the first step, we use haloperidol as the blocking agent to investigate the binding specificity of the radiotracers to the  $\sigma_1$  receptors *in vivo*. With administration of haloperidol (0.1 mL, 1 mg/kg) 5 min prior to [ $^{18}\text{F}$ ]**19** injection, significant reduction of the accumulation of radiotracer in organs known to contain  $\sigma_1$  receptors was observed. A marked reduction of 58% in the brain was comparable to that obtained with [ $^{18}\text{F}$ ]**6b** (62% reduction at 60 min)<sup>31</sup> and [ $^{11}\text{C}$ ]**1** (60–70% reduction at 30 min).<sup>46</sup> These data suggest the specific binding of [ $^{18}\text{F}$ ]**19** to  $\sigma_1$  receptors *in vivo*. On the other hand, [ $^{18}\text{F}$ ]**23** displayed lower brain uptake and relatively fast washout compared with [ $^{18}\text{F}$ ]**19**, which may result from the lower lipophilicity and lower affinity of [ $^{18}\text{F}$ ]**23** for  $\sigma_1$  receptors. Little reduction of radiotracer accumulation in organs known to contain  $\sigma_1$  receptors was observed, reflecting that [ $^{18}\text{F}$ ]**23** is not suitable for further

investigation owing to its lower affinity ( $K_i = 37.5$  nM) for  $\sigma_1$  receptors.

It is well-known that haloperidol binds with similarly high affinity to dopamine  $D_2/D_3$  receptors and  $\sigma_1$  receptors.<sup>47,48</sup> Haloperidol also binds adrenergic and serotonergic receptors with moderate affinity.<sup>49</sup> Furthermore, the reduced metabolite of haloperidol has high affinity for  $\sigma_1$  and  $\sigma_2$  receptors while showing much lower affinity for dopamine receptors than haloperidol itself.<sup>50</sup> As indicated in the literature, **1** had low affinity or no affinity for 36 other receptors, ion channels, and second messenger systems.<sup>23</sup> Therefore, **1** was synthesized in our laboratory and used as a better  $\sigma_1$  receptor ligand for demonstrating the specificity of [ $^{18}\text{F}$ ]**19** to  $\sigma_1$  receptors *in vivo*. Significant reduction in radiotracer uptake in organs known to contain  $\sigma_1$  receptors, including the brain, heart, lungs, kidneys, and spleen, was observed by pretreatment of animals with different concentrations of **1** (2, 5, or 10  $\mu\text{mol}/\text{kg}$ ). Because our aim is to develop a  $\sigma_1$  receptor brain imaging agent, interaction of [ $^{18}\text{F}$ ]**19** with other receptors in the brain needs to be considered. It was reported that **1** has high affinity for EBP ( $K_i = 1.72$  nM)<sup>51</sup> and for VACHT ( $K_i = 50.2$  nM).<sup>52</sup> Our ligand **19** displayed 799 times lower affinity for VACHT with a  $K_i$  value of  $631 \pm 50.2$  nM. To further investigate the specific binding of [ $^{18}\text{F}$ ]**19** to  $\sigma_1$  receptors in the brain, tamoxifen, (*S*)-(-)-raclopride, and fluvoxamine were used as blocking agents to investigate the possible interaction of [ $^{18}\text{F}$ ]**19** with EBP, dopamine  $D_2/D_3$  receptors, and 5-HTT. It was encouraging that pretreatment of tamoxifen, (*S*)-(-)-raclopride, and fluvoxamine resulted in no significant reduction in radiotracer accumulation in the brain. Thus, [ $^{18}\text{F}$ ]**19** does not bind to EBP, dopamine  $D_2/D_3$  receptors, and 5-HTT in the brain at the low

doses used for imaging. These data indicated that [ $^{18}\text{F}$ ]19 accumulation in the mouse brain could represent specific binding to  $\sigma_1$  receptors.

To evaluate the potential use of [ $^{18}\text{F}$ ]19 for imaging  $\sigma_1$  receptor density in the brain, we performed an ex vivo autoradiography study to investigate the accumulation of [ $^{18}\text{F}$ ]19 in different brain regions in Sprague–Dawley rats. [ $^{18}\text{F}$ ]19 accumulated in brain areas known to have high expression of  $\sigma_1$  receptors, such as the cortex, cerebellum, and thalamus. The rank order of [ $^{18}\text{F}$ ]19 uptake in various brain regions is in good agreement with that of [ $^{11}\text{C}$ ]1.<sup>40</sup> To further evaluate [ $^{18}\text{F}$ ]19 as a promising radiotracer for investigating  $\sigma_1$  receptors in living subjects, microPET/CT studies were carried out in anaesthetized Sprague–Dawley rats. [ $^{18}\text{F}$ ]19 crossed the BBB rapidly and accumulated in the midbrain, thalamus, hypothalamus, cortex, pontine reticular nucleus, and cerebellum, which are known to contain high expression of  $\sigma_1$  receptors, while lower uptakes were observed in the areas with negligible levels of  $\sigma_1$  receptors. It should be pointed out that the brain regional distribution of [ $^{18}\text{F}$ ]19 evaluated by microPET was slightly different from that of ex vivo autoradiography studies, which may result from the different conditions of the animals (awake vs anesthetized).<sup>53,54</sup> Pretreatment with haloperidol resulted in the reduction of radiotracer accumulation in all brain regions, consistent with the results from the biodistribution study. Taken together, these results suggest that the novel radiotracer [ $^{18}\text{F}$ ]19 may be useful for quantitative imaging of  $\sigma_1$  receptors in vivo.

Another important point for development of a brain radiotracer is to investigate the radioligand's metabolism profile in vivo. If radiolabeled metabolites could enter the brain, they would confound the binding signals in the brain. Therefore, studies of the in vitro metabolism of compound 19 by rat liver microsomes and in vivo metabolic fate of [ $^{18}\text{F}$ ]19 in the brain and liver of male ICR mice at 30 min were carried out. The results showed that the parent compound [ $^{18}\text{F}$ ]19 was the only radioactive species present in the mouse brain, indicating no entry of radioactive metabolites into the brain.

In conclusion, the novel radiotracer [ $^{18}\text{F}$ ]19 warrants further evaluation as a promising imaging agent for investigation of the  $\sigma_1$  receptors in humans.

## EXPERIMENTAL SECTION

**General Procedures.** All reagents and solvents were obtained from commercial sources and used without further purification unless otherwise stated. Tamoxifen (Toronto Research Chemicals Inc., Canada) was purchased from J & K Scientific Ltd. Haloperidol, (S)-(-)-raclopride (+)-tartrate salt and fluvoxamine maleate were obtained from Sigma-Aldrich Co. Ltd. (Beijing, China). Compound 1 was synthesized according to the method in the literature with some modifications.<sup>55</sup> The synthetic route and characterization are shown in the Supporting Information.  $^1\text{H}$  NMR spectra were recorded on a Bruker Avance III (400 MHz) instrument. Chemical shifts are reported as  $\delta$  (ppm) relative to tetramethylsilane ( $s$  = singlet,  $br$   $s$  = broad singlet,  $d$  = doublet,  $dd$  = double doublet,  $t$  = triplet,  $m$  = multiplet).  $^{13}\text{C}$  NMR spectra were recorded on a Bruker Avance III (100 MHz) spectrometer. MS spectra were obtained with a Quattro micro API ESI/MS instrument (Waters, United States). High-resolution mass spectrometry (HRMS) was performed on a JEOL-NMS-SX102 spectrometer (JEOL). Melting points were measured on a SGW X-4 micro melting point apparatus (Shanghai Precision Scientific Instrument Co., Ltd., China). Elemental analyses (C, H, N) were determined on an Elementar 240C device (PerkinElmer, United States). X-ray crystallography data were collected on a Bruker Smart Apex II crystal diffractometer (Bruker Co., Germany). Reactions were

monitored by thin-layer chromatography (TLC) (TLC silica gel 60 F<sub>254</sub>, E. Merck). Flash column chromatography was performed on silica gel (200–400 mesh) using the solvent system indicated. Elemental analysis and HPLC methods were used to determine the purity of the test compounds that were used for the binding assay. All the final compounds were tested with a purity of more than 95% (Supporting Information).

HPLC analyses were performed on a Waters 600 system (Waters Corp., United States) equipped with a Waters 2489 UV–vis detector and a Raytest Gabi NaI(Tl) scintillation detector (Raytest, Germany). Analyses were carried out on an Agela Venusil MP C18 column (250  $\times$  4.6 mm, 5  $\mu\text{m}$ ) using acetonitrile (0.1% TFA)/water (0.1% TFA) (50:50) as the mobile phase at a flow rate of 1 mL/min. Semipreparative HPLC separations were performed on a Shimadzu SCL-20AVP system consisting of a binary pump with an online degasser, a model SPD-20AVP UV–vis detector operating at a wavelength of 254 nm, and a Bioscan Flow Count 3200 NaI/PMT  $\gamma$ -radiation scintillation detector. Samples were separated on an Alltech Alltima RPC-18 column (250 mm  $\times$  10 mm, 5  $\mu\text{m}$ ) using acetonitrile (0.1% TFA)/water (0.1% TFA) (60:40) as the mobile phase at a flow rate of 4 mL/min.

The UPLC–MS/MS system consisted of a Waters Acquity UPLC system equipped with an Acquity ethylene-bridged (BEH) C18 column (2.1  $\times$  55 mm, 1.7  $\mu\text{m}$ ) and a mass spectrometer. The mass spectrometric detection was performed using a Quattro micro triple quadrupole instrument and an electrospray ionization (ESI) interface in positive ionization mode. The capillary voltage was set at 3.0 kV. The source temperature was 110  $^\circ\text{C}$ , and the desolvation temperature was maintained at 500  $^\circ\text{C}$ . Nitrogen was used both as a cone gas and as a desolvation gas, with flow rates of 30 and 600 L/h, respectively. Argon was used as a collision gas. Data processing was performed with the Mass Lynx 4.1 software.

ICR mice (male, 4 weeks old, 18–22 g) and Sprague–Dawley rats (male, 9 weeks old, 220–250 g) were purchased from the Laboratory Animal Centre of the Peking University Health Science Centre (Beijing, China). All animal experiments were approved by the Institutional Animal Care and Use Committee of Beijing Normal University and performed in compliance with relevant laws and institutional guidelines.

**Chemistry.** 6-(2-Fluoroethoxy)nicotinaldehyde (11). To a solution of 6-chloronicotinaldehyde (200.0 mg, 1.4 mmol) in DMF (10 mL) were added 2-fluoroethanol (360.0 mg, 5.6 mmol) and *t*-BuOK (320.0 mg, 2.8 mmol). The mixture was stirred at rt for 6 h, poured into water, and extracted with  $\text{CHCl}_3$ . The combined organic layers were dried ( $\text{Na}_2\text{SO}_4$ ), filtered, and evaporated. Flash chromatography on silica gel (hexane:ethyl acetate = 5:1) gave 11 as a white solid (55.0 mg, 23%). Mp: 48–49  $^\circ\text{C}$ .  $^1\text{H}$  NMR (400 MHz,  $\text{CDCl}_3$ ):  $\delta$  (ppm) 9.97 ( $s$ , 1H), 8.62 ( $d$ ,  $J$  = 2.1 Hz, 1H), 8.10 ( $dd$ ,  $J_1$  = 8.6 Hz,  $J_2$  = 2.3 Hz, 1H), 6.93 ( $d$ ,  $J$  = 8.7 Hz, 1H), 4.86–4.83 ( $m$ , 1H), 4.74–4.71 ( $m$ , 2H), 4.67–4.65 ( $m$ , 1 H). ESI-MS:  $[\text{M} + \text{H}]^+$  ( $m/z$  = 170.1).

1'-(4-Fluorobenzyl)-3H-spiro[2-benzofuran-1,4'-piperidine] (17). To a solution of 8 (160.0 mg, 0.85 mmol) in MeCN (10 mL) were added  $\text{K}_2\text{CO}_3$  (1.17 g, 8.5 mmol), KI (133.0 mg, 0.85 mmol), and 1-(bromomethyl)-4-fluorobenzene (160.0 mg, 0.85 mmol). The mixture was refluxed for 8 h. After filtration, the solvent was removed in vacuo and the residue purified by silica gel chromatography (hexane:ethyl acetate = 4:1) to provide 17 as a white solid (75.0 mg, 30%). Mp: 61–62  $^\circ\text{C}$ .  $^1\text{H}$  NMR (400 MHz,  $\text{CDCl}_3$ ):  $\delta$  (ppm) 7.35–7.32 ( $m$ , 2H), 7.28–7.26 ( $m$ , 2H), 7.21–7.19 ( $m$ , 1H), 7.16–7.14 ( $m$ , 1H), 7.04–6.99 ( $m$ , 2H), 5.07 ( $s$ , 2H), 3.56 ( $s$ , 2H), 2.84 ( $s$ , 1H), 2.81 ( $s$ , 1H), 2.42 ( $t$ ,  $J$  = 11.6 Hz, 2H), 1.99 ( $br$   $s$ , 2H), 1.78 ( $s$ , 1H), 1.75 ( $s$ , 1H).  $^{13}\text{C}$  NMR (100 MHz,  $\text{CDCl}_3$ ):  $\delta$  163.23, 160.79, 145.71, 138.95, 130.77, 130.69, 127.55, 127.33, 121.05, 120.80, 115.10, 114.89, 84.70, 70.72, 62.61, 50.06, 36.62. ESI-MS:  $[\text{M} + \text{H}]^+$  ( $m/z$  = 298.0).

1'-(4-Methoxybenzyl)-3H-spiro[2-benzofuran-1,4'-piperidine] (18). To a solution of 8 (500.0 mg, 2.64 mmol) in  $\text{CH}_3\text{CN}$  (5 mL) were added 1-(bromomethyl)-4-methoxybenzene (580.0 mg, 2.90 mmol),  $\text{K}_2\text{CO}_3$  (2.0 g, 14.5 mmol), and KI (200.0 mg, 1.20 mmol). The mixture was stirred at rt for 1 h. After filtration, the solvent was removed in vacuo and the residue purified by silica gel chromatog-

raphy (hexane:ethyl acetate = 1:2) to provide **18** as a white solid (300.0 mg, 40%). Mp: 76–77 °C. <sup>1</sup>H NMR (400 MHz, CDCl<sub>3</sub>): δ (ppm) 7.30–7.24 (m, 4H), 7.22–7.19 (m, 1H), 7.16–7.14 (m, 1H), 6.88 (d, *J* = 9.2 Hz, 2H), 5.07 (s, 2H), 3.81 (s, 3H), 3.55 (s, 2H), 2.86 (s, 1H), 2.84 (s, 1H), 2.41 (t, *J* = 11.2 Hz, 2H), 2.03 (br s, 2H), 1.78–1.74 (m, 2H). ESI-MS: [M + H]<sup>+</sup> (*m/z* = 309.7). Anal. Calcd for C<sub>20</sub>H<sub>23</sub>NO<sub>2</sub>: C, 77.64; H, 7.49; N, 4.53. Found: C, 77.66; H, 7.51; N, 4.50.

**1'-(4-(2-Fluoroethoxy)benzyl)-3H-spiro[2-benzofuran-1,4'-piperidine] (19)**. Compound **8** (267.8 mg, 1.42 mmol) was dissolved in anhydrous THF (18.8 mL) under a N<sub>2</sub> atmosphere, followed by addition of NaH (120.3 mg, 5.00 mmol). The mixture was stirred at rt for 15 min, followed by addition of **10** (330.1 mg, 1.42 mmol). The mixture was then stirred at rt for an additional 15 h, poured into water, and extracted with CH<sub>2</sub>Cl<sub>2</sub>. The combined organic layers were dried (MgSO<sub>4</sub>), filtered, and evaporated in vacuo. Purification by silica gel chromatography (CH<sub>2</sub>Cl<sub>2</sub>:CH<sub>3</sub>OH = 20:1) gave **19** (276.0 mg, 57%) as a white solid. The solid was crystallized from a mixture of diethyl ether and petroleum ether as white crystals. Mp: 52–53 °C. <sup>1</sup>H NMR (400 MHz, CDCl<sub>3</sub>): δ (ppm) 7.37 (d, *J* = 8.5 Hz, 2H), 7.29–7.25 (m, 2H), 7.21–7.18 (m, 2H), 6.92 (d, *J* = 8.6 Hz, 2H), 5.06 (s, 2H), 4.82 (t, *J* = 4.1 Hz, 1H), 4.70 (t, *J* = 4.1 Hz, 1H), 4.25 (t, *J* = 4.1 Hz, 1H), 4.18 (t, *J* = 4.1 Hz, 1H), 3.71 (s, 2H), 3.01 (s, 1H), 3.00 (s, 1H), 2.61 (t, *J* = 10.9 Hz, 2H), 2.21 (br s, 2H), 1.80 (s, 1H), 1.77 (s, 1H). <sup>13</sup>C NMR (100 MHz, CDCl<sub>3</sub>): δ 157.58, 145.84, 138.98, 130.53, 127.51, 127.30, 121.02, 120.81, 114.41, 84.80, 82.78, 81.09, 70.68, 67.28, 67.08, 62.77, 50.04, 36.66. ESI-MS: [M + H]<sup>+</sup> (*m/z* = 341.7). Anal. Calcd for C<sub>21</sub>H<sub>24</sub>FNO<sub>2</sub>·1/2H<sub>2</sub>O: C, 71.98; N, 4.00; H, 7.19. Found: C, 71.49; N, 3.50; H, 7.15.

**1'-((6-(2-Fluoroethoxy)pyridin-3-yl)methyl)-3H-spiro[2-benzofuran-1,4'-piperidine] (20)**. To a solution of **11** (50.0 mg, 0.29 mmol) in 1,2-dichloroethane (10 mL) was added compound **8** (50.0 mg, 0.26 mmol). The mixture was reacted for 2 h, followed by addition of NaBH(OAc)<sub>3</sub> (65.0 mg, 0.42 mmol). The mixture was reacted for another 6 h. Then the reaction was quenched with saturated NaHCO<sub>3</sub>, and the solvent was removed in vacuo. Following extraction with ethyl acetate, the combined organic layers were dried (Na<sub>2</sub>SO<sub>4</sub>) and filtered, and the solvent was removed in vacuo. The residue was purified by silica gel chromatography (hexane:ethyl acetate = 1:1) to give **20** as a white solid (52.0 mg, 58%). Mp: 73–74 °C. <sup>1</sup>H NMR (400 MHz, CDCl<sub>3</sub>): δ (ppm) 8.05 (s, 1H), 7.66–7.64 (m, 1H), 7.28–7.26 (m, 2H), 7.21–7.19 (m, 1H), 7.15–7.14 (m, 1H), 6.80 (d, *J* = 8.5 Hz, 1H), 5.07 (s, 2H), 4.82 (t, *J* = 4.0 Hz, 1H), 4.70 (t, *J* = 4.0 Hz, 1H), 4.60 (t, *J* = 4.4 Hz, 1H), 4.53 (t, *J* = 4.3 Hz, 1H), 3.52 (s, 2H), 2.83 (s, 1H), 2.80 (s, 1H), 2.42 (t, *J* = 10.6 Hz, 2H), 1.97 (br s, 2H), 1.78 (s, 1H), 1.75 (s, 1H). <sup>13</sup>C NMR (100 MHz, CDCl<sub>3</sub>): δ 162.63, 147.00, 145.63, 140.22, 138.95, 127.59, 127.36, 121.07, 120.80, 110.96, 84.61, 82.11, 81.27, 70.75, 64.86, 64.66, 59.90, 49.96, 36.59. HRMS (EI): *m/z* calcd for C<sub>20</sub>H<sub>24</sub>FN<sub>2</sub>O<sub>2</sub> [M + H]<sup>+</sup> 343.1822, found 343.1832.

**4-((3H-Spiro[2-benzofuran-1,4'-piperidine]-1'-yl)methyl)phenol (21)**. Compound **8** (500.0 mg, 2.64 mmol) was dissolved in 1,2-dichloroethane (15 mL) under a N<sub>2</sub> atmosphere, followed by addition of 4-hydroxybenzaldehyde (355.0 mg, 2.89 mmol), and the mixture was stirred at rt for 2 h. Then NaBH(OAc)<sub>3</sub> (650.0 mg, 3.07 mmol) was added, and the mixture was stirred for an additional 6 h. Then the reaction was quenched with saturated NaHCO<sub>3</sub>, evaporated to remove the organic solvent, and extracted with ethyl acetate. The combined organic layers were dried (MgSO<sub>4</sub>) and filtered, and the solvent was removed in vacuo. Then the residue was purified by silica gel chromatography (CH<sub>2</sub>Cl<sub>2</sub>:CH<sub>3</sub>OH = 5:1) to provide **21** as a white solid (539.6 mg, 69%). Mp: 192–194 °C. <sup>1</sup>H NMR (400 MHz, CDCl<sub>3</sub>): δ (ppm) 9.34 (s, 1H), 7.26 (s, 4H), 7.13 (d, *J* = 7.5 Hz, 2H), 6.73 (d, *J* = 8.0 Hz, 2H), 4.96 (s, 2H), 3.37 (s, 2H), 2.75 (s, 2H), 2.33 (s, 2H), 1.89 (br s, 2H), 1.62 (s, 1H), 1.59 (s, 1H). ESI-MS: [M + H]<sup>+</sup> (*m/z* = 295.7).

**1'-(4-(2-(2-Fluoroethoxy)ethoxy)benzyl)spiro[2-benzofuran-1-(3H),4'-piperidine] (22)**. A mixture of **21** (88.0 mg, 0.30 mmol), 2-(2-fluoroethoxy)ethyl 4-methylbenzenesulfonate (**15**) (130 mg, 0.47 mmol), and potassium carbonate (138.0 mg, 1 mmol) in CH<sub>3</sub>CN (5 mL) was refluxed for 6 h. After the solvent was removed in vacuo, the

residue was purified by silica gel chromatography (hexane:ethyl acetate = 1:1) to provide **22** as a yellow oil (120.0 mg, 67%). <sup>1</sup>H NMR (400 MHz, CDCl<sub>3</sub>): δ (ppm) 7.28–7.23 (m, 4H), 7.21–7.18 (m, 1H), 7.15–7.13 (m, 1H), 6.89 (d, *J* = 8.5 Hz, 2H), 5.06 (s, 2H), 4.65 (t, *J* = 4.1 Hz, 1H), 4.53 (t, *J* = 4.1 Hz, 1H), 4.16–4.13 (m, 2H), 3.90–3.88 (m, 2H), 3.87–3.85 (m, 1H), 3.80–3.78 (m, 1H), 3.54 (s, 2H), 2.85 (s, 1H), 2.82 (s, 1H), 2.42 (t, *J* = 11.6 Hz, 2H), 2.02–1.97 (m, 2H), 1.77 (s, 1H), 1.74 (s, 1H). <sup>13</sup>C NMR (100 MHz, CDCl<sub>3</sub>): δ 157.91, 145.78, 138.97, 130.59, 127.54, 127.34, 121.04, 120.86, 114.41, 84.78, 84.02, 82.34, 77.19, 70.73, 70.51, 70.00, 67.52, 62.79, 50.03, 36.59. ESI-MS: [M + H]<sup>+</sup> (*m/z* = 386.1).

**1'-(4-(2-(2-(2-Fluoroethoxy)ethoxy)ethoxy)benzyl)spiro[2-benzofuran-1-(3H),4'-piperidine] (23)**. The procedure described for the synthesis of **22** was applied to **16** to give **23** as a yellow oil (74%). <sup>1</sup>H NMR (400 MHz, CDCl<sub>3</sub>): δ (ppm) 7.27–7.23 (m, 4H), 7.20–7.18 (m, 1H), 7.15–7.13 (m, 1H), 6.88 (d, *J* = 8.5 Hz, 2H), 5.06 (s, 2H), 4.62 (t, *J* = 4.1 Hz, 1H), 4.50 (t, *J* = 4.1 Hz, 1H), 4.13 (t, *J* = 4.9 Hz, 2H), 3.86 (t, *J* = 4.9 Hz, 2H), 3.79 (t, *J* = 4.1 Hz, 1H), 3.75–3.71 (m, 5H), 3.53 (s, 2H), 2.85 (s, 1H), 2.82 (s, 1H), 2.41 (t, *J* = 11.6 Hz, 2H), 2.06–1.93 (m, 2H), 1.77 (s, 1H), 1.74 (s, 1H). <sup>13</sup>C NMR (100 MHz, CDCl<sub>3</sub>): δ 157.95, 145.79, 138.97, 130.52, 127.53, 127.32, 121.03, 120.84, 114.36, 84.79, 84.00, 82.32, 70.89, 70.72, 70.57, 70.37, 69.86, 67.45, 62.81, 50.03, 36.60. ESI-MS: [M + H]<sup>+</sup> (*m/z* = 430.2).

**2-(4-((3H-Spiro[2-benzofuran-1,4'-piperidin]-1'-yl)methyl)phenoxy)ethyl 4-Methylbenzenesulfonate (24)**. Compound **21** (150.0 mg, 0.51 mmol) was added to a solution of 1,2-bis(4-methylbenzenesulfonate) (**12**) (563.9 mg, 1.524 mmol) in acetonitrile (10 mL), followed by K<sub>2</sub>CO<sub>3</sub> (70.0 mg, 0.51 mmol). The mixture was refluxed for 12 h, then poured into water, and extracted with CH<sub>2</sub>Cl<sub>2</sub>. The combined organic layers were dried (Na<sub>2</sub>SO<sub>4</sub>) and filtered, and the solvent was removed in vacuo. The residue was purified by silica gel chromatography (CH<sub>2</sub>Cl<sub>2</sub>:CH<sub>3</sub>OH = 10:1) to provide **24** as a white solid (169 mg, 67%). Mp: 90–92 °C. <sup>1</sup>H NMR (400 MHz, CDCl<sub>3</sub>): δ (ppm) 7.82 (d, *J* = 8.3 Hz, 2H), 7.34 (d, *J* = 8.1 Hz, 2H), 7.28–7.24 (m, 4H), 7.22–7.15 (m, 2H), 6.75 (d, *J* = 8.4 Hz, 2H), 5.06 (s, 2H), 4.38–4.35 (m, 2H), 4.15–4.13 (m, 2H), 3.53 (s, 2H), 2.80 (br s, 2H), 2.45–2.35 (m, 5H), 2.04–1.98 (m, 2H), 1.77 (s, 1H), 1.74 (s, 1H). ESI-MS: [M + H]<sup>+</sup> (*m/z* = 493.6).

**2-(2-(2-(4-((3H-Spiro[2-benzofuran-1,4'-piperidin]-1'-yl)methyl)phenoxy)ethoxy)ethoxy)ethyl 4-Methylbenzenesulfonate (25)**. The procedure described for the synthesis of **24** was applied to **15** to give **25** as a yellow oil (61%). <sup>1</sup>H NMR (400 MHz, CDCl<sub>3</sub>): δ (ppm) 7.80 (d, *J* = 8.2 Hz, 2H), 7.32 (d, *J* = 8.1 Hz, 2H), 7.27–7.24 (m, 4H), 7.20–7.18 (m, 1H), 7.16–7.12 (m, 1H), 6.88 (d, *J* = 8.3 Hz, 2H), 5.06 (s, 2H), 4.17–4.15 (m, 2H), 4.11–4.09 (m, 2H), 3.83–3.80 (m, 2H), 3.71–3.80 (m, 2H), 3.67–3.65 (m, 2H), 3.62–3.60 (m, 2H), 3.53 (s, 2H), 2.85 (s, 1H), 2.82 (s, 1H), 2.43–2.38 (m, 5H), 2.01–1.96 (m, 2H), 1.77 (s, 1H), 1.74 (s, 1H). ESI-MS: [M + H]<sup>+</sup> (*m/z* = 582.1).

**X-ray Crystallography.** Single-crystal X-ray diffraction measurements were carried out on a Bruker Smart Apex II crystal diffractometer at 150(2) K using graphite-monochromated Mo K $\alpha$  radiation ( $\lambda$  = 0.71073 Å). An empirical absorption correction was applied using the SADABS program.<sup>56</sup> All structures were solved by direct methods and refined by full-matrix least-squares on *F*<sup>2</sup> using the SHELXL-97 program package.<sup>57</sup> All of the hydrogen atoms (except solvent H<sub>2</sub>O) were geometrically fixed using the riding model.

**In Vitro Binding Assays.  $\sigma$  Receptor Binding Assays.** Radioligand competition binding assays were performed with rat brain homogenates for  $\sigma_1$  receptors and rat liver homogenates for  $\sigma_2$  receptors.<sup>37</sup> For  $\sigma_1$  receptors, (+)-[<sup>3</sup>H]pentazocine was employed as the competing radioligand. For  $\sigma_2$  receptors, the nonselective radioligand [<sup>3</sup>H]-1,3-di-*o*-tolylguanidine (DTG) was used in the presence of 10  $\mu$ M dextralorphan for selective masking of  $\sigma_1$  receptor binding. Non-specific binding was determined with 10  $\mu$ M haloperidol. *K*<sub>i</sub> values were calculated according to the Cheng–Prusoff equation and represent the mean  $\pm$  standard deviation (SD) from at least three independent experiments, each performed in triplicate.

**VACHT Binding Assays.** Radioligand competition binding assays were performed using membrane homogenates obtained from PC12 cells stably transfected with rat VACHT (obtained from Ali Roghani,

Department of Pharmacology and Neuroscience, Texas Tech University Health Sciences Center, Lubbock, TX) and (–)-[<sup>3</sup>H]-vesamicol (1 nM working concentration). Assays were performed with compound **19** (at concentrations of 10<sup>–11</sup> to 10<sup>–5</sup> mol/L) in 50 mM Tris–HCl, pH 7.4, by incubation at room temperature for 120 min. Nonspecific binding was determined in the presence of 10 μM (–)-vesamicol. *K<sub>i</sub>* values were calculated according to the Cheng–Prusoff equation and represent the mean from two single experiments, each performed in triplicate.

**Radiochemistry.** 1'-(4-(2-[<sup>18</sup>F]Fluoroethoxy)benzyl)-3H-spiro[2-benzofuran-1,4'-piperidine] ([<sup>18</sup>F]**19**). [<sup>18</sup>F]fluoride was produced via the <sup>18</sup>O (p,n) <sup>18</sup>F nuclear reaction with 20 MeV protons in a Sumitomo HM-20PS cyclotron and transferred into a reaction vessel containing a solution of Kryptofix 2.2.2 (13 mg) and K<sub>2</sub>CO<sub>3</sub> (1.1 mg) in MeCN/water (0.8 mL/0.2 mL). The solvent was removed at 115 °C under a stream of nitrogen gas, and the residue was azeotropically dried with 1.0 mL of anhydrous acetonitrile, repeated three times. A solution of the corresponding tosylate precursor **24** (3.0 mg) in MeCN (1.0 mL) was added to the reaction vessel. The mixture was heated at 95 °C for 5 min, diluted with water (20 mL), and passed through a C-18 Sep-Pak cartridge. The crude product was eluted off the cartridge with MeCN (1 mL) and the solution loaded onto a semipreparative HPLC column for purification (Alltech Alltima RPC-18, 250 × 10 mm, 5 μm, eluent 60% CH<sub>3</sub>CN and 40% water with 0.1% TFA, flow rate 4 mL/min). The total synthesis time was about 1 h. The radiochemical yield was 35–60% (*n* = 5, decay corrected), and the specific activity at the end of synthesis was 30–55 GBq/μmol, determined with an HPLC-based method. For animal experiments, the radiotracer was formulated as a saline solution containing no more than 8% ethanol.

1'-(4-(2-(2-[<sup>18</sup>F]Fluoroethoxy)ethoxy)ethoxy)benzyl)spiro[2-benzofuran-1(3H),4'-piperidine] ([<sup>18</sup>F]**23**). The procedure described for the synthesis of [<sup>18</sup>F]**19** was applied to **25** to give [<sup>18</sup>F]**23**. The total synthesis time was about 1 h. The radiochemical yield was 20–40% (*n* = 3, decay corrected). The radiochemical purity was >99%. The specific activity at the end of the synthesis was 30–55 GBq/μmol, determined with an HPLC-based method. For animal experiments, the radiotracer was formulated as a saline solution containing no more than 8% ethanol.

To identify the radiotracer, [<sup>18</sup>F]**19** and [<sup>18</sup>F]**23** were coinjected and coeluted with the corresponding unlabeled compounds (Shimadzu SCL-20AVP, Agela Venusil MP C18, 250 mm × 4.6 mm, 5 μm). Their HPLC profiles using acetonitrile (0.1% TFA)/water (0.1% TFA) (50:50, v/v) at a flow rate of 1 mL/min are presented in the Supporting Information (Figure S2). The retention times of unlabeled **19** and [<sup>18</sup>F]**19** were observed to be 5.31 and 5.83 min, respectively. The retention times of unlabeled **23** and [<sup>18</sup>F]**23** were observed to be 4.81 and 5.30 min, respectively. The difference in retention time was in good agreement with the time lag, which corresponds to the volume and flow rate within the distance between the UV and radioactivity detector of our HPLC system.

**Determination of the Partition Coefficient.** Partition coefficients for [<sup>18</sup>F]**19** and [<sup>18</sup>F]**23** were determined by measuring the distribution of the radiotracers between 1-octanol and sodium phosphate buffer (PBS, 0.05 M, pH 7.4). The radiolabeled compound (370 kBq, 10 μL) was mixed with 1-octanol (3.0 mL) and sodium phosphate buffer (3.0 mL) in a centrifuge tube. The tube was vortexed for 3 min at room temperature, followed by centrifugation at 3500 rpm for 5 min. About 50 μL of the 1-octanol layer was weighed in a tared tube. The 1-octanol layer was removed, and about 0.5 mL of the buffer layer was weighed in a second tared tube. After addition of 0.5 mL of buffer to the 1-octanol fraction and 0.05 mL of 1-octanol to the aqueous fraction, activity in both tubes was measured in an automatic γ-counter (Wallac 1470 Wizard, United States). The log *D* value was calculated by comparing the ratio of the cpm/mL of 1-octanol to that of PBS and expressed as log *D* = log[cpm/mL(1-octanol)/cpm/mL(PBS)]. Samples from the remaining organic layer were repartitioned until consistent distribution coefficient values were obtained. The measurement was carried out in triplicate and repeated three times.

**In Vitro Stability of [<sup>18</sup>F]**19**.** [<sup>18</sup>F]**19** (3.7 MBq, in 100 μL of water) was added to 80% EtOH (1 mL) or 0.9% sodium chloride (1 mL). The solutions were vortexed and then allowed to stand at room temperature for 4 h. To test the plasma stability, [<sup>18</sup>F]**19** was added to the freshly prepared murine plasma (1 mL), and the solution was incubated at 37 °C for 4 h. The radiochemical purity of [<sup>18</sup>F]**19** in the solutions was assayed by HPLC at 1, 2, and 4 h.

**Biological Experiments. Biodistribution Studies in Male ICR Mice and Blocking Studies.** Four groups of ICR mice (*n* = 5 in each group) were injected intravenously with a saline solution of [<sup>18</sup>F]**19** or [<sup>18</sup>F]**23** (370 kBq, 0.1 mL). The mice were sacrificed by decapitation at 2, 30, 60, and 120 min postinjection. Whole brain, heart, lungs, liver, spleen, and other organs of interest were removed, weighed, and counted in an automatic γ-counter. The percentage of injected dose per gram of wet tissue (% ID/g) was calculated by a comparison of the tissue counts to suitably diluted aliquots of the injected material. All radioactivity measurements were corrected for decay. Averages and SD were calculated.

For the initial blocking studies, the mice were injected via tail vein with either saline (0.1 mL) or haloperidol (0.1 mL, 1.0 mg/kg) 5 min prior to [<sup>18</sup>F]**19** or [<sup>18</sup>F]**23** injection. Sixty minutes after radiotracer administration, the animals were sacrificed by decapitation. Tissues of interest were excised and analyzed as described. Significant differences between control and test groups were determined by Student's *t* test (independent, two-tailed). The criterion for significance was *p* ≤ 0.05.

For the further blocking studies, ICR male mice were injected via tail vein with either saline (0.1 mL) or a blocking agent, including **1** (0.1 mL, 2 μmol/kg), **1** (0.1 mL, 5 μmol/kg), **1** (0.1 mL, 10 μmol/kg), haloperidol (0.1 mL, 2.2 μmol/kg), **1** (0.1 mL, 2.2 μmol/kg), (S)-(–)-raclopride (0.1 mL, 2.2 μmol/kg), fluvoxamine (0.1 mL, 2.2 μmol/kg), or tamoxifen (0.1 mL, 2.2 μmol/kg), 5 min prior to the injection of [<sup>18</sup>F]**19** (0.1 mL, 370 kBq). Sixty minutes after radiotracer administration, the animals were sacrificed by decapitation. Tissues of interest were excised and analyzed as described. Significant differences between control and test groups were determined by Student's *t* test (independent, two-tailed). The criterion for significance was *p* ≤ 0.05.

**Ex Vivo Autoradiography.** A solution of [<sup>18</sup>F]**19** (0.2 mL, 12.2 MBq) was intravenously injected into conscious Sprague–Dawley rats (*n* = 3). The rat was killed by cervical dislocation 60 min after injection of the radioligand. The brain was removed and frozen in a liquid nitrogen bath, and coronal brain sections (20 μm) were cut on a cryostat microtome (CM1900, Leica, Germany). The brain slices were dried at room temperature and were exposed to an imaging plate (PerkinElmer, United States) for 2 h. Autoradiographic images were obtained using a phosphor imaging system (CyclonePlus, PerkinElmer, United States) and analyzed with the AIDA 2.31 software (Raytest, Straubenhardt, Germany).

**MicroPET Imaging Experiment.** The Sprague–Dawley rats were anesthetized with isoflurane (1.5–2.5%) in oxygen at a flow rate of 1–2 L/min and injected with 23 MBq of [<sup>18</sup>F]**19** (0.2 mL in saline) via tail vein. Blocking studies involved preinjection with haloperidol (0.2 mL, 1 mg/kg) 5 min prior to tracer administration. MicroPET imaging was performed on an eXplore VISTA-CT scanner (GE Healthcare, Spain) equipped with a computer-controlled bed. The field of view (FOV) was 6.8 cm transaxial and 4.8 cm axial with an image resolution of <1 mm. Imaging data were acquired for 30 min, starting 60 min after tracer injection, followed by a 5 min CT scan for anatomical information. For image reconstruction, list-mode data were sorted into 3-D sinograms, transformed by Fourier rebinning, and reconstructed by 2-D ordered-subset expectation maximization reconstruction with 2 iterations and 50 subsets. Corrections for dead time, random scattering, and attenuation were made for each scan.

**In Vitro Metabolism Studies of **19** in Liver Microsomes.** Unlabeled compound **19** was incubated with rat liver microsomes. The incubation mixture consisted of 2 mg of protein/mL of liver microsomes, 100 μM **19**, and an NADPH-generating system with 2 mM β-NADPH, 20 mM glucose 6-phosphate, 2 U of glucose 6-phosphate dehydrogenase, and 12 mM MgCl<sub>2</sub>·12H<sub>2</sub>O, all in 0.05 M Tris–HCl buffer (pH 7.4). The total volume was 500 μL. The reaction was started by the addition of **19** after preincubation of the reaction

mixture for 3 min at 37 °C. Blank incubations were performed in the absence of **19**. The reaction was stopped after 30 min by the addition of 1.5 mL of ice-cold methanol. The reaction mixture was vortexed and centrifuged at 15000 g for 15 min. The supernatant was collected and filtered through a 0.22 μm microbore cellulose membrane, and aliquots were analyzed by UPLC–MS.

**In Vivo Radiometabolic Stability of [<sup>18</sup>F]**19**.** The mice were administered intravenously with [<sup>18</sup>F]**19** (18.5 MBq, 0.2 mL) and sacrificed 30 min after tracer injection. The brain and liver were collected and washed with saline. The samples were placed separately in 2 mL of ice-cooled phosphate-buffered saline (0.01 M, pH 7.4) and homogenized for 2 min with a LabGEN 7 homogenizer. Ice-cold MeCN (4 mL) was added to the homogenates, and the mixtures were vortexed first and then centrifuged at 13 200 rpm for 5 min. The supernatants were collected and passed through a 0.22 mm Millipore filter. The filtrates were concentrated to 0.2 mL under a stream of nitrogen gas flow and then injected onto the radio-HPLC system (Waters 600 system, Agela Venusil MP C18, 250 mm × 4.6 mm, 5 μm) for analysis using a flow rate of 1 mL/min, and the eluent was acetonitrile (0.1% TFA)/water (0.1% TFA) (45:55, v/v).

## ■ ASSOCIATED CONTENT

### ● Supporting Information

Purity of key target compounds, HPLC chromatograms of **19**, [<sup>18</sup>F]**19**, **23**, and [<sup>18</sup>F]**23**, HPLC analysis of the stability of [<sup>18</sup>F]**19** in vitro, X-ray crystallographic data for compound **19** (including a CIF file), and synthetic route and characterization of compound **1**. This material is available free of charge via the Internet at <http://pubs.acs.org>.

## ■ AUTHOR INFORMATION

### Corresponding Author

\*Phone: +86-10-58808891. Fax: +86-10-58808891. E-mail: [hmjia@bnu.edu.cn](mailto:hmjia@bnu.edu.cn).

### Notes

The authors declare no competing financial interest.

## ■ ACKNOWLEDGMENTS

We give special thanks to Dr. Xuebing Deng (College of Chemistry, Beijing Normal University) for assistance with the X-ray diffraction. We are grateful to Prof. Henry Huang for his helpful suggestions and valuable comments on this manuscript. This work was supported by the National Natural Science Foundation of China (Grant 21071023).

## ■ ABBREVIATIONS USED

AD, Alzheimer's disease; DMF, dimethylformamide; EBP, emopamil binding protein; NADPH, nicotinamide adenine dinucleotide phosphate; PBS, phosphate-buffered saline; PET, positron emission tomography; PD, Parkinson's disease; RCP, radiochemical purity; SSRI, selective serotonin reuptake inhibitor; 5-HTT, serotonin transporter; SPECT, single-photon emission computed tomography; TBAF, tetra-*n*-butylammonium fluoride; TFA, trifluoroacetic acid; THF, tetrahydrofuran; TLC, thin-layer chromatography; VACHT, vesicular acetylcholine transporter

## ■ REFERENCES

- (1) Hanner, M.; Moebius, F. F.; Flandorfer, A.; Knaus, H. G.; Striessnig, J.; Kempner, E.; Glossmann, H. Purification, molecular cloning, and expression of the mammalian sigma<sub>1</sub>-binding site. *Proc. Natl. Acad. Sci. U. S. A.* **1996**, *93*, 8072–8077.
- (2) Aydar, E.; Palmer, C. P.; Klyachko, V. A.; Jackson, M. B. The sigma receptor as a ligand-regulated auxiliary potassium channel subunit. *Neuron* **2002**, *34*, 399–410.

- (3) Hayashi, T.; Su, T. P. Sigma-1 receptor chaperones at the ER-mitochondrion interface regulate Ca<sup>2+</sup> signaling and cell survival. *Cell* **2007**, *131*, 596–610.

- (4) Walker, J. M.; Bowen, W. D.; Walker, F. O.; Matsumoto, R. R.; De Costa, B.; Rice, K. C. Sigma receptors: biology and function. *Pharmacol. Rev.* **1990**, *42*, 355–402.

- (5) Mei, J.; Pasternak, G. W. Molecular cloning and pharmacological characterization of the rat sigma<sub>1</sub> receptor. *Biochem. Pharmacol.* **2001**, *62*, 349–355.

- (6) Kim, F. J.; Kovalyshyn, I.; Burgman, M.; Neilan, C.; Chien, C. C.; Pasternak, G. W. Sigma 1 receptor modulation of G-protein-coupled receptor signaling: potentiation of opioid transduction independent from receptor binding. *Mol. Pharmacol.* **2010**, *77*, 695–703.

- (7) Guitart, X.; Codony, X.; Monroy, X. Sigma receptors: biology and therapeutic potential. *Psychopharmacology* **2004**, *174*, 301–319.

- (8) Hayashi, T.; Tsai, S. Y.; Mori, T.; Fujimoto, M.; Su, T. P. Targeting ligand-operated chaperone sigma-1 receptors in the treatment of neuropsychiatric disorders. *Expert Opin. Ther. Targets* **2011**, *15*, 557–577.

- (9) Maurice, T.; Su, T. P. The pharmacology of sigma-1 receptors. *Pharmacol. Ther.* **2009**, *124*, 195–206.

- (10) Feher, A.; Juhasz, A.; Laszlo, A.; Kalman, J., Jr.; Pakaski, M.; Kalman, J.; Janka, Z. Association between a variant of the sigma-1 receptor gene and Alzheimer's disease. *Neurosci. Lett.* **2012**, *517*, 136–139.

- (11) Ishikawa, M.; Hashimoto, K. The role of sigma-1 receptors in the pathophysiology of neuropsychiatric diseases. *J. Recept. Ligand Channel Res.* **2010**, *3*, 25–36.

- (12) Van Waarde, A.; Rybczynska, A. A.; Ramakrishnan, N.; Ishiwata, K.; Elsinga, P. H.; Dierckx, R. A. Sigma receptors in oncology: therapeutic and diagnostic applications of sigma ligands. *Curr. Pharm. Des.* **2010**, *16*, 3519–3537.

- (13) Megalizzi, V.; Le Mercier, M.; Decaestecker, C. Sigma receptors and their ligands in cancer biology: overview and new perspectives for cancer therapy. *Med. Res. Rev.* **2012**, *32*, 410–427.

- (14) Ito, K.; Hirooka, Y.; Matsukawa, R.; Nakano, M.; Sunagawa, K. Decreased brain sigma-1 receptor contributes to the relationship between heart failure and depression. *Cardiovasc. Res.* **2012**, *93*, 33–40.

- (15) Mishina, M.; Ishiwata, K.; Ishii, K.; Kitamura, S.; Kimura, Y.; Kawamura, K.; Oda, K.; Sasaki, T.; Sakayori, O.; Hamamoto, M.; Kobayashi, S.; Katayama, Y. Function of sigma<sub>1</sub> receptors in Parkinson's disease. *Acta Neurol. Scand.* **2005**, *112*, 103–107.

- (16) Mishina, M.; Ohyama, M.; Ishii, K.; Kitamura, S.; Kimura, Y.; Oda, K.; Kawamura, K.; Sasaki, T.; Kobayashi, S.; Katayama, Y.; Ishiwata, K. Low density of sigma<sub>1</sub> receptors in early Alzheimer's disease. *Ann. Nucl. Med.* **2008**, *22*, 151–156.

- (17) Toyohara, J.; Sakata, M.; Ishiwata, K. Imaging of sigma<sub>1</sub> receptors in the human brain using PET and [<sup>11</sup>C]SA4503. *Cent. Nerv. Syst. Agents Med. Chem.* **2009**, *9*, 190–196.

- (18) Ishikawa, M.; Sakata, M.; Ishii, K.; Kimura, Y.; Oda, K.; Toyohara, J.; Wu, J.; Ishiwata, K.; Iyo, M.; Hashimoto, K. High occupancy of sigma<sub>1</sub> receptors in the human brain after single oral administration of donepezil: a positron emission tomography study using [<sup>11</sup>C]SA4503. *Int. J. Neuropsychopharmacol.* **2009**, *12*, 1127–1131.

- (19) Sakata, M.; Kimura, Y.; Naganawa, M.; Oda, K.; Ishii, K.; Chihara, K.; Ishiwata, K. Mapping of human cerebral sigma<sub>1</sub> receptors using positron emission tomography and [<sup>11</sup>C]SA4503. *NeuroImage* **2007**, *35*, 1–8.

- (20) Waterhouse, R.; Nobler, M.; Chang, R.; Zhou, Y.; Morales, O.; Kuwabara, H. First evaluation of the sigma-1 receptor radioligand [<sup>18</sup>F] 1–3-fluoropropyl-4-((4-cyanophenoxy)-methyl) piperidine ([<sup>18</sup>F] FPS) in healthy humans. *NeuroImage* **2004**, *22*, T29–T30.

- (21) Waterhouse, R. N.; Chang, R. C.; Atuehene, N.; Collier, T. L. In vitro and in vivo binding of neuroactive steroids to the sigma-1 receptor as measured with the positron emission tomography radioligand [<sup>18</sup>F]FPS. *Synapse* **2007**, *61*, 540–546.

- (22) Stone, J. M.; Arstad, E.; Erlandsson, K.; Waterhouse, R. N.; Ell, P. J.; Pilowsky, L. S. [<sup>123</sup>I]TPCNE—a novel SPET tracer for the sigma-1 receptor: first human studies and in vivo haloperidol challenge. *Synapse* **2006**, *60*, 109–117.
- (23) Matsuno, K.; Nakazawa, M.; Okamoto, K.; Kawashima, Y.; Mita, S. Binding properties of SA4503, a novel and selective  $\sigma_1$  receptor agonist. *Eur. J. Pharmacol.* **1996**, *306*, 271–279.
- (24) Maier, C. A.; Wünsch, B. Novel spiro-piperidines as highly potent and subtype selective sigma-receptor ligands. Part 1. *J. Med. Chem.* **2002**, *45*, 438–448.
- (25) Maier, C. A.; Wünsch, B. Novel sigma receptor ligands. Part 2. SAR of spiro[[2]benzopyran-1,4'-piperidines] and spiro[[2]-benzofuran-1,4'-piperidines] with carbon substituents in position 3. *J. Med. Chem.* **2002**, *45*, 4923–4930.
- (26) Wiese, C.; Grosse Maestrup, E.; Schepmann, D.; Vela, J. M.; Holenz, J.; Buschmann, H.; Wünsch, B. Pharmacological and metabolic characterisation of the potent  $\sigma_1$  receptor ligand 1'-benzyl-3-methoxy-3H-spiro[[2]benzofuran-1,4'-piperidine]. *J. Pharm. Pharmacol.* **2009**, *61*, 631–640.
- (27) Grosse Maestrup, E.; Wiese, C.; Schepmann, D.; Hiller, A.; Fischer, S.; Scheunemann, M.; Brust, P.; Wünsch, B. Synthesis of spirocyclic  $\sigma_1$  receptor ligands as potential PET radiotracers, structure-affinity relationships and in vitro metabolic stability. *Bioorg. Med. Chem.* **2009**, *17*, 3630–3641.
- (28) Wiese, C.; Grosse Maestrup, E.; Schepmann, D.; Grimme, S.; Humpf, H. U.; Brust, P.; Wünsch, B. Enantioselective  $\sigma_1$  receptor binding and biotransformation of the spirocyclic PET tracer 1'-benzyl-3-(3-fluoropropyl)-3H-spiro[[2]benzofuran-1,4'-piperidine]. *Chirality* **2011**, *23*, 148–154.
- (29) Maisonial, A.; Grosse Maestrup, E.; Fischer, S.; Hiller, A.; Scheunemann, M.; Wiese, C.; Schepmann, D.; Steinbach, J.; Deuther-Conrad, W.; Wünsch, B.; Brust, P. A <sup>18</sup>F-labeled fluorobutyl-substituted spirocyclic piperidine derivative as a selective radioligand for PET imaging of sigma<sub>1</sub> receptors. *ChemMedChem* **2011**, *6*, 1401–1410.
- (30) Maestrup, E. G.; Fischer, S.; Wiese, C.; Schepmann, D.; Hiller, A.; Deuther-Conrad, W.; Steinbach, J.; Wünsch, B.; Brust, P. Evaluation of spirocyclic 3-(3-fluoropropyl)-2-benzofurans as  $\sigma_1$  receptor ligands for neuroimaging with positron emission tomography. *J. Med. Chem.* **2009**, *52*, 6062–6072.
- (31) Fischer, S.; Wiese, C.; Maestrup, E. G.; Hiller, A.; Deuther-Conrad, W.; Scheunemann, M.; Schepmann, D.; Steinbach, J.; Wünsch, B.; Brust, P. Molecular imaging of sigma receptors: synthesis and evaluation of the potent  $\sigma_1$  selective radioligand [<sup>18</sup>F]fluspidine. *Eur. J. Nucl. Med. Mol. Imaging* **2011**, *38*, 540–551.
- (32) Maisonial, A.; Grosse Maestrup, E.; Wiese, C.; Hiller, A.; Schepmann, D.; Fischer, S.; Deuther-Conrad, W.; Steinbach, J.; Brust, P.; Wünsch, B. Synthesis, radiofluorination and pharmacological evaluation of a fluoromethyl spirocyclic PET tracer for central  $\sigma_1$  receptors and comparison with fluoroalkyl homologs. *Bioorg. Med. Chem.* **2012**, *20*, 257–269.
- (33) Chen, R. Q.; Li, Y.; Zhang, Q. Y.; Jia, H. M.; Deuther-Conrad, W.; Schepmann, D.; Steinbach, J.; Brust, P.; Wünsch, B.; Liu, B. L. Synthesis and biological evaluation of a radioiodinated spiro-piperidine ligand as a potential  $\sigma_1$  receptor imaging agent. *J. Labelled Compd. Radiopharm.* **2010**, *53*, 569–574.
- (34) Kubota, H.; Fujii, M.; Ikeda, K.; Takeuchi, M.; Shibamura, T.; Isomura, Y. Spiro-substituted piperidines as neurokinin receptor antagonists. I. Design and synthesis of (±)-N-[2-(3,4-dichlorophenyl)-4-(spiro [isobenzofuran-1(3H), 4'-piperidin]-1'-yl)butyl]-N-methylbenzamide, YM-35375, as a new lead compound for novel neurokinin receptor antagonists. *Chem. Pharm. Bull.* **1998**, *46*, 351–354.
- (35) Wang, X.; Li, Y.; Deuther-Conrad, W.; Xie, F.; Chen, X.; Cui, M. C.; Zhang, X. J.; Zhang, J. M.; Steinbach, J.; Brust, P.; Liu, B. L.; Jia, H. M. Synthesis and biological evaluation of <sup>18</sup>F labeled fluoro-oligo-ethoxylated 4-benzylpiperazine derivatives for sigma-1 receptor imaging. *Bioorg. Med. Chem.* **2013**, *21*, 215–222.
- (36) Holtke, C.; von Wallbrunn, A.; Kopka, K.; Schober, O.; Heindel, W.; Schafers, M.; Bremer, C. A fluorescent photoprobe for the imaging of endothelin receptors. *Bioconjugate Chem.* **2007**, *18*, 685–694.
- (37) Fan, C. Y.; Jia, H. M.; Deuther-Conrad, W.; Brust, P.; Steinbach, J.; Liu, B. L. Novel <sup>99m</sup>Tc labeled  $\sigma_1$  receptor ligand as a potential tumor imaging agent. *Sci. China, Ser. B: Chem.* **2006**, *49*, 169–176.
- (38) Sorger, D.; Scheunemann, M.; Grossmann, U.; Fischer, S.; Vercouille, J.; Hiller, A.; Wenzel, B.; Roghani, A.; Schliebs, R.; Brust, P.; Sabri, O.; Steinbach, J. A new <sup>18</sup>F-labeled fluoroacetylmorpholino derivative of vesamicol for neuroimaging of the vesicular acetylcholine transporter. *Nucl. Med. Biol.* **2008**, *35*, 185–195.
- (39) *OECD Guidelines for Testing of Chemicals*; OECD Publishing: Paris, France, 1989; <http://www.oecd.org/dataoecd/17/36/1948177.pdf>.
- (40) Kawamura, K.; Ishiwata, K.; Tajima, H.; Ishii, S.; Matsuno, K.; Homma, Y.; Senda, M. In vivo evaluation of [<sup>11</sup>C]SA4503 as a PET ligand for mapping CNS sigma<sub>1</sub> receptors. *Nucl. Med. Biol.* **2000**, *27*, 255–261.
- (41) Fishback, J. A.; Robson, M. J.; Xu, Y. T.; Matsumoto, R. R. Sigma receptors: potential targets for a new class of antidepressant drug. *Pharmacol. Ther.* **2010**, *127*, 271–282.
- (42) Rack, E.; Frohlich, R.; Schepmann, D.; Wünsch, B. Design, synthesis and pharmacological evaluation of spirocyclic  $\sigma_1$  receptor ligands with exocyclic amino moiety (increased distance 1). *Bioorg. Med. Chem.* **2011**, *19*, 3141–3151.
- (43) Glennon, R. A. Pharmacophore identification for sigma-1 ( $\sigma_1$ ) receptor binding: application of the “deconstruction–reconstruction–elaboration” approach. *Mini-Rev. Med. Chem.* **2005**, *5*, 927–940.
- (44) Laruelle, M.; Slifstein, M.; Huang, Y. Relationships between radiotracer properties and image quality in molecular imaging of the brain with positron emission tomography. *Mol. Imaging Biol.* **2003**, *5*, 363–375.
- (45) Patel, S.; Gibson, R. In vivo site-directed radiotracers: a mini-review. *Nucl. Med. Biol.* **2008**, *35*, 805–815.
- (46) Kawamura, K.; Ishiwata, K.; Shimada, Y.; Kimura, Y.; Kobayashi, T.; Matsuno, K.; Homma, Y.; Senda, M. Preclinical evaluation of [<sup>11</sup>C]SA4503: radiation dosimetry, in vivo selectivity and PET imaging of sigma<sub>1</sub> receptors in the cat brain. *Ann. Nucl. Med.* **2000**, *14*, 285–292.
- (47) Leysen, J. E.; Janssen, P. M.; Gommeren, W.; Wynants, J.; Pauwels, P. J.; Janssen, P. A. In vitro and in vivo receptor binding and effects on monoamine turnover in rat brain regions of the novel antipsychotics risperidone and ocapridone. *Mol. Pharmacol.* **1992**, *41*, 494–508.
- (48) Malmberg, A.; Mikael, A.; Mohell, N. Agonist and inverse agonist activity at the dopamine D<sub>3</sub> receptor measured by guanosine 5'-[ $\gamma$ -thio]triphosphate-[<sup>35</sup>S] binding. *J. Pharmacol. Exp. Ther.* **1998**, *285*, 119–126.
- (49) Kroeze, W. K.; Hufeisen, S. J.; Popadak, B. A.; Renock, S. M.; Steinberg, S.; Ernsberger, P.; Jayathilake, K.; Meltzer, H. Y.; Roth, B. L. H1-histamine receptor affinity predicts short-term weight gain for typical and atypical antipsychotic drugs. *Neuropsychopharmacology* **2003**, *28*, 519–526.
- (50) Cobos, E. J.; del Pozo, E.; Baeyens, J. M. Irreversible blockade of sigma-1 receptors by haloperidol and its metabolites in guinea pig brain and SH-SY5Y human neuroblastoma cells. *J. Neurochem.* **2007**, *102*, 812–825.
- (51) Berardi, F.; Ferorelli, S.; Colabufo, N. A.; Leopoldo, M.; Perrone, R.; Tortorella, V. A multireceptorial binding reinvestigation on an extended class of sigma ligands: N-[omega-(indan-1-yl) and tetralin-1-yl]alkyl] derivatives of 3,3-dimethylpiperidine reveal high affinities towards  $\sigma_1$  and EBP sites. *Bioorg. Med. Chem.* **2001**, *9*, 1325–1335.
- (52) Shiba, K.; Ogawa, K.; Ishiwata, K.; Yajima, K.; Mori, H. Synthesis and binding affinities of methylvesamicol analogs for the acetylcholine transporter and sigma receptor. *Bioorg. Med. Chem.* **2006**, *14*, 2620–2626.

(53) Elfving, B.; Bjornholm, B.; Knudsen, G. M. Interference of anaesthetics with radioligand binding in neuroreceptor studies. *Eur. J. Nucl. Med. Mol. Imaging* **2003**, *30*, 912–915.

(54) Zhao, F.; Jin, T.; Wang, P.; Kim, S. G. Isoflurane anesthesia effect in functional imaging studies. *NeuroImage* **2007**, *38*, 3–4.

(55) Kawamura, K.; Elsinga, P. H.; Kobayashi, T.; Ishii, S.; Wang, W. F.; Matsuno, K.; Vaalburg, W.; Ishiwata, K. Synthesis and evaluation of  $^{11}\text{C}$ - and  $^{18}\text{F}$ -labeled 1-[2-(4-alkoxy-3-methoxyphenyl)ethyl]-4-(3-phenylpropyl)piperazines as sigma receptor ligands for positron emission tomography studies. *Nucl. Med. Biol.* **2003**, *30*, 273–284.

(56) Sheldrick, G. *SADABS, Program for Empirical Absorption Correction of Area Detector Data*; University of Göttingen: Göttingen, Germany, 1996.

(57) Sheldrick, G. M. *SHELXL-97, Program for the Refinement of Crystal Structure from Direction Data*; University of Göttingen: Göttingen, Germany, 1997.